Modeling of Fiber Kinking in Composite Laminates

Delft University of Technology
December 1, 2015

Modeling of Fiber Kinking in Composite Laminates

by

René R. R. da Costa

in partial fulfillment of the requirements for the degree of

Master of Science
in Civil Engineering

at the Delft University of Technology,
to be defended publicly on December, 08 2015.

Thesis committee:	prof. dr. ir. L. J. Sluys	(Chairman)
	dr. ir. F. P. van der Meer	(Supervisor)
	dr. ir. A. M. Aragón	
	ir. L. J. M. Houben	

Acknowledgments

This document presents an overview of the work carried out during my MSc-thesis at the University of Technology Delft and is the culmination of my Master of Science program. Before proceeding to lengthy derivations and mathematical concepts I would like to take this opportunity to thank those without whom this thesis would not have been possible.
I would like to thank my committee members prof.dr.ir. L.J. Sluys and dr.ir. F.P. van der Meer who introduced me to the subject of computational mechanics and provided me with valuable advise and insights throughout my thesis and for their patience with my limited programming skills.
To my colleagues in room 6.54 thanks for the great working environment and keeping it entertaining during my time in 6.54 and of-course for the free coffee.
I would also like to thank my friends and family for their constant and at times irritating support and encouragement, especially in times when it was sincerely needed.

René da Costa
Delft, December 2015

Abstract

Recent advancements in computational methods has led to improvements in the computational modeling of tensile failure of composite laminates. Models for compressive failure however, have not yet reached the same level of maturity. Particularly in the case of fiber kinking there is a need for improved modeling techniques. Fiber kinking occurs when fiber imperfection combined with matrix failure lead to localized deformation in a band of finite width (kink bands). Current computational models have focused on micro-level, where matrix and fibers are modeled independently. The various experimental and analytical research on fiber kinking has lead to numerous failure criteria and analytical models for kink bands. The collapse response of kink bands however, has yet to be incorporated in a meso-level computational model. A step is required to translate these micro-mechanical and analytical models to a meso-level framework and improve the state of the art of compressive failure modeling of composite laminates.

In this thesis an attempt is made at transitioning from a micro to a meso-level failure model for fiber kinking. A discontinuous approach is proposed for modeling kink bands. The kink bands are represented as strong discontinuities in the displacement field using the phantom node method. With this method the angle of failure propagation can be easily controlled. The discontinuities are introduced after violation of a stress-based failure criterion and therefore necessitates the use of an initially rigid cohesive law to incorporate the kink band response. To construct such a law a shifted formulation is used, meaning, the law is derived with a finite initial stiffness and shifted to achieve the initially rigid behavior. Strong discontinuity analysis and a discrete micro-mechanical model are used to derive two separate cohesive models in the local kink band coordinate frame, while a simplified approach is also applied to derive a third model in the discontinuity coordinate frame.

The nonlinear characteristics and bifurcation of the models necessitate the use of a capable solution algorithm that will follow the true equilibrium path. Therefore the crack opening displacement arclength method is used to; indirectly control direction of crack growth, pass the bifurcation point and capture possible snap-back behavior. Additionally an adaptive time stepping strategy is applied to increase efficiency and robustness.

The model and algorithm have been implemented in a one dimensional framework using Timoshenko beam elements and verified against an analytical solution. The local models have shown to capture the trends derived using the analytical solution well, with the strong discontinuity model being the most accurate. The simplified approach however fails to properly account for these trends.

The current work has resulted in an initial step towards a meso-level computational model of fiber kinking. It is shown that the discontinuous approach provides a good representation of kink bands provided that a proper cohesive model is used that incorporates both material and geometrical parameters influencing kink bands.

Contents

Chapter 1: Introduction

1.1. Context of study

The use of computational tools in analyzing structural behavior has become common practice for the modern day engineer. With the rise of new high performance engineered materials, researchers continuously work on developing and improving computational methods to facilitate exploitation of these materials in engineering practices.

Composite laminates are a set of such high performance materials. *Laminate* refers to the layered structure of the material and *composite*, in this case refers to the fact that each layer (or ply) consists of a fiber material (e.g. glass or carbon) surrounded by a polymer matrix (e.g. epoxy). Composite laminates present many advantages compared to traditional structural material such as; a high strength and stiffness to weight ratio and the ability to tailor their mechanical properties to specific application needs. The laminates derive their properties mostly from the fiber material and their orientation within the plies, the matrix serves to keep the fibers together. Within a ply the fibers can be long and evenly distributed, in one or multiple directions, or fibers can be short and randomly distributed. In this thesis only unidirectional plies are considered, i.e. the fibers are long and oriented in one direction within a ply.

From the definition of the composite laminates it is clear that different observation scales can be identified (see fig. 1.1):
micro-level, where fibers and matrix are independently recognizable and the material is non homogeneous.
meso-level, where each ply is independently recognizable and the ply itself can be seen as an orthotropic homogeneous material.
macro-level, where the total composite can be treated as anisotropic homogeneous material.
In this thesis, the observation scale is set at a meso-level.

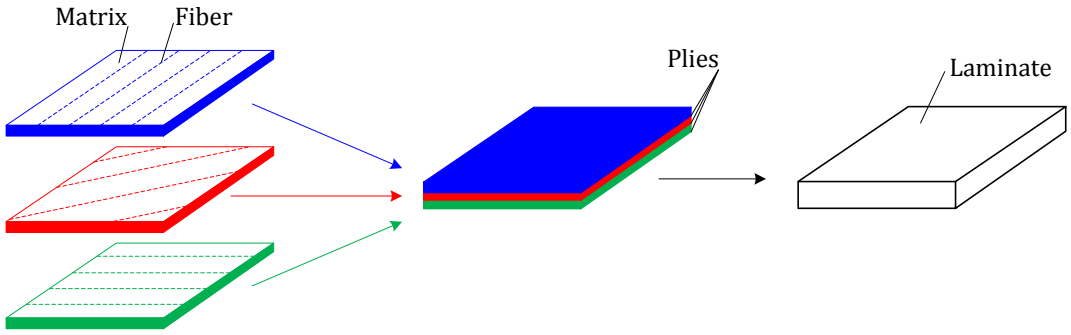

Figure 1.1: Observation scales, from left to right: micro-level, meso-level, macro-level.

Composite laminates as structural material have traditionally been applied in the automotive and aerospace industries and are slowly being introduced into the civil engineering sector. The difficulty in predicting the reliability of a composite structure however, has led to the use of high safety factors and extensive testing for certification making their usage less efficient. This

has hindered a more widespread exploitation of composites in various engineering sectors. The development of robust and reliable computational models for analysis of composite laminates would significantly improve the use of the material and reduce certification costs. A complicating factor in development of computational models is that a combination of different failure mechanisms may occur (as can be seen in fig. 1.2) causing a complex failure process. Typical failure mechanisms that have been distinguished for composite laminates are: fiber fracture, fiber kinking, matrix cracking, fiber-matrix debonding and delamination.

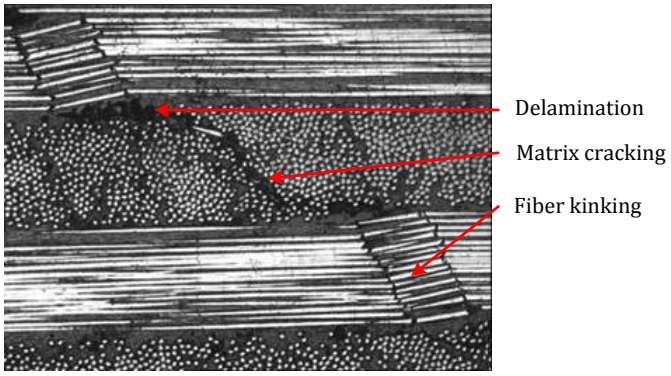

Figure 1.2: Experimental observation of different failure mechanisms [24].

1.2. Problem definition

As mentioned in the previous section robust computational methods are needed for analysis of composite laminates to allow for more efficient exploitation of the material. Recent works by van der Meer [31] have resulted in meso-level computational models for the analysis of composite laminates. These models focused on tensile failure modes of composite laminates however, for a complete failure analysis compressive failure modes must also be addressed. To that end the case of fiber kinking has been found to be the dominant failure mechanism governing composite laminates under longitudinal compression [25].

Throughout the years significant micro-scale research has been conducted on this topic increasing the knowledge on the compressive behavior of composites and resulting in numerous micro-mechanical models. However, there is still a need for translation of these micro models to a meso-level framework for a complete failure analysis.

1.2.1. Thesis goals

The main goal of this thesis is to study the fiber kinking failure mode and develop a computational meso-level model to simulate both the pre- and post-failure behavior of a composite laminate failing by fiber kinking. The thesis goal can be summarized in the following research question:

How can the failure behavior of a composite ply failing by fiber kinking be incorporated into meso-level computational models for composite laminates?

1.2.2. Objectives

The objectives of this thesis can be summarized as follows:

- Determine an appropriate mechanical model for simulation of fiber kinking at meso-level
- Derive the necessary mathematical formulations
- Implement derivations into 1D model
- Qualitatively asses models failure behavior
- Improve efficiency and robustness of model

1.3. Report outline

In the remainder of this chapter the necessary numerical framework is introduced along with several computational failure models. In Chapter 2 the various works conducted on the subject of fiber kinking are reviewed and a description of the governing mechanisms behind fiber kinking is presented. In Chapter 3 the model outline is presented along with the mathematical derivation. Next, in Chapter 4 the numerical implementation is briefly discussed and the model is tested and validated against an analytical solution. Finally, in Chapter 5 the overall conclusion of the thesis is presented along with an outlook on future developments.

1.4. The finite element method

The model developed in this thesis is executed within the framework of the finite element method. A brief introduction of the method is presented here, for more in-depth information on the finite element method the reader is referred to the many textbooks on this subject such as [33].

The finite element method is a method for solving partial differential equations in the primary unknowns. In its current application the primary unknowns are the displacement fields and the partial differential equations are the static equilibrium equations. The solution is approximated by solving a discretized weak form of the equilibrium equations denoted by eq. (1.1).

$$\mathbf{f}_{\text{int}} = \mathbf{f}_{\text{ext}} \tag{1.1}$$

Where $\mathbf{f}_{\text{ext}}$ represents the external force vector containing the applied forces to the system and $\mathbf{f}_{\text{int}}$ is the internal force vector which is a function of the displacement field. The displacement field is discretized by dividing the problem domain in a finite number of elements, interconnected by nodes, with each their own set of degrees of freedom and shape functions. The shape functions are defined such that the degrees of freedom can be interpreted as nodal displacements. With the definition of the shape function matrix $\mathbf{N}$ and the nodal displacement vector $\mathbf{a}$, the displacement field $\mathbf{u} = (u_x, u_y, u_z)^T$ is expressed by eq. (1.2).

$$\mathbf{u}(\mathbf{x}) = \mathbf{N}(\mathbf{x})\mathbf{a} \tag{1.2}$$

The strain fields are defined as:

$$\boldsymbol{\varepsilon}(\mathbf{x}) = \mathbf{B}(\mathbf{x})\mathbf{a} = \mathbf{L}\mathbf{N}(\mathbf{x})\mathbf{a} \tag{1.3}$$

with $\mathbf{L}$ being the matrix containing the differential operators.

For linear elastic material behavior the stresses $\boldsymbol{\sigma}$ are related to the strain field $\boldsymbol{\varepsilon}$ via the relation:

$$\boldsymbol{\sigma} = \mathbf{D}\boldsymbol{\varepsilon} \tag{1.4}$$

Where the matrix $\mathbf{D}$ represents the material tangent,

$$\mathbf{D} = \frac{\partial \boldsymbol{\sigma}}{\partial \boldsymbol{\varepsilon}} \tag{1.5}$$

With eqs. (1.3) and (1.4) the stress field can be computed from the (history of) nodal displacements. The internal force vector can then be evaluated from the stress field in a loop over the elements. Equation (1.1) can then be written in the well known form:

$$\mathbf{K}\mathbf{a} = \mathbf{f}_{\text{ext}} \tag{1.6}$$

with

$$\mathbf{K} = \int_{\Omega} \mathbf{B}^T \mathbf{D} \mathbf{B} \mathrm{d}\Omega \tag{1.7}$$

It must be noted that within the finite element method integration is carried out numerically and in most cases using Gaussian integration schemes.

When non-linearities are present, as is the case in this thesis, the left hand side of eq. (1.1) becomes a non-linear function of $\mathbf{a}$ and eqs. (1.4) to (1.7) are no longer valid. The solution is now sought in an incremental fashion and a *fictitious* time variable is introduced so that eq. (1.1) must now be solved for each time step. Due to the non-liniearities however eq. (1.1) cannot be solved directly therefore the solution is sought iteratively with the Newton-Raphson procedure. This procedure solves a linearized system in every iteration and the solution vector is updated in every iteration with eq. (1.8) until the convergence norm eq. (1.11) is reached. Subsequently a new increment is added and the process is restarted.

$$\mathbf{a}_j = \mathbf{a}_{j-1} + \mathbf{K}_{j-1}^{-1} \mathbf{r}(\mathbf{a}) \tag{1.8}$$

with

$$\mathbf{K}_{j-1}^{-1} = \left. \frac{\partial \mathbf{f}_{\text{int}}}{\partial \mathbf{a}} \right|_{\mathbf{a}=\mathbf{a}_{j-1}} \tag{1.9}$$

and

$$\mathbf{r}(\mathbf{a}) = \mathbf{f}_{\text{ext}}^{\text{t}+\Delta\text{t}} - \mathbf{f}_{\text{int}}(\mathbf{a}_{j-1}) \tag{1.10}$$

until

$$\frac{\|\mathbf{r}\|}{\|\mathbf{r}\|_0} \leq \epsilon_{\min} \tag{1.11}$$

Where $\|\mathbf{r}\|_0$ is the norm of the residual vector from the first iteration.

1.5. Computational failure models

Several methods exist to model failure of materials, in this section some of these methods are shortly reviewed. The methods can be divided into two categories: continuum approaches and discontinuous approaches. In continuum approaches failure is smeared over a band with a finite width and causes a weakening of the element response. Contrary to continuum approaches discontinuous approaches introduce discontinuities in or between elements creating a new interior boundary rather then just weakening the element response.

1.5.1. Continuum models

Continuum models fit directly into the framework of the finite element method discussed in section 1.4. These models account for material failure by adjusting the relation between stress and stain and therefore the material tangent. Because failure is smeared over a band of finite width, continuum approaches often suffer from mesh sensitivity. Regularization techniques introducing internal length scales have been implemented to reduce mesh sensitivity, however, this does not always completely solve the mesh sensitivity problem.

Plasticity Plasticity models are one of the most used non-linear material models in finite element modeling. The main idea in plasticity models is that the strains can be decomposed in an elastic strain and a permanent (plastic) strain. The constitutive relation is then given by:

$$\boldsymbol{\sigma} = \mathbf{D}^{\mathbf{e}}(\boldsymbol{\varepsilon} - \boldsymbol{\varepsilon}^{\boldsymbol{p}}) \tag{1.12}$$

Typically, the plastic strain is an unknown variable and is computed such that a certain yield criterion is satisfied. The yield criterion is usually formulated in terms of the stresses making eq. (1.12) an iterative equation. For modeling of failure, the stress criterion can be formulated such that the stress must vanish upon increasing plastic strain.

Damage Continuum damage models (CDM) offer a more straightforward approach to failure modeling. In CDM failure is seen as a gradual reduction in stiffness following a certain damage evolution law. The constitutive relation is given by:

$$\boldsymbol{\sigma} = (1 - \omega)\mathbf{D}^{\mathbf{e}}\boldsymbol{\varepsilon} \tag{1.13}$$

where ω represents the damage variable. Generally the stiffness reduction is computed explicitly giving CDM an advantage over plasticity models. However, when unloading is addressed plasticity formulation unload via the initial elastic stiffness whereas in CDM unloading occurs via a secant stiffness resulting in no permanent straining.

1.5.2. Discontinuous models

Discontinuous methods traditionally are applied when a discontinuity in the displacement field is expected as a result of failure. These methods however require a change in the finite element formulation as the kinematical relations must be adapted to account for the discontinuity in the displacement field. Common discontinuous methods include: interface elements and the extended finite element method (XFEM). Interface elements require the location of the discontinuity to be known prior to failure which is not preferred when modeling fiber kinking and therefore will not be considered here. XFEM does offer the flexibility to model discontinuity without prior knowledge of failure location. The partition of unity method and the phantom node method are both variation of XFEM. In the current context the methods are equivalent however, the phantom node method presents a simpler implementation. Therefore only the latter is further discussed.

Phantom node method The phantom node method developed by Hansbo and Hansbo [14] offers a relatively simple way of introducing discontinuities in elements without having to change the topology of the elements.

In the phantom node method an element that is crossed by a crack Γ_k is subdivided into two domains Ω^+ and Ω^-. The discontinuity in the element displacement field is constructed by adding *phantom* nodes over the existing nodes and replacing the cracked element by two partially active, overlapping elements with independent displacement fields. The connectivity and active parts can bee seen in fig. 1.3.

The active parts of the elements are represented by the definition of the displacement field shown in eq. (1.14)

$$\mathbf{u}(\mathbf{x}) = \begin{cases} \mathbf{N}(\mathbf{x})\mathbf{u}^+, & \mathbf{x} \in \Omega^+ \\ \mathbf{N}(\mathbf{x})\mathbf{u}^-, & \mathbf{x} \in \Omega^- \end{cases} \tag{1.14}$$

with $\mathbf{N}$ the standard finite element shape functions, the strain field is derived from the displacement field in the common fashion.

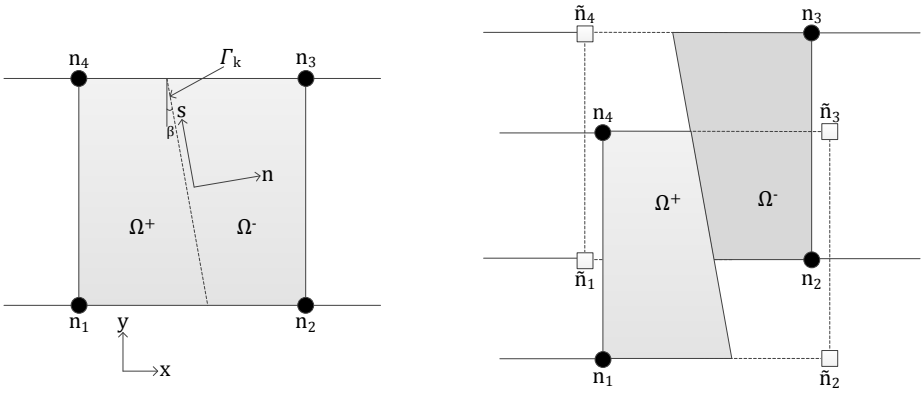

Figure 1.3: Connectivity and active parts of two overlapping elements in phantom node method.

The displacement jump over the crack is defined as the difference in the displacement fields of the two initially overlapping elements.

$$[\![\mathbf{u}]\!](\mathbf{x}) = \mathbf{N}(\mathbf{x})(\mathbf{u}^+ - \mathbf{u}^-),\ \mathbf{x} \in \Gamma_k \tag{1.15}$$

In a local frame the displacement jump can be expressed in a normal and shear component as:

$$[\![\hat{\mathbf{u}}]\!] = ([\![u_n]\!]; [\![u_s]\!])^T = \mathbf{Q}[\![\mathbf{u}]\!] \tag{1.16}$$

with $\mathbf{Q}$ the rotation matrix:

$$\mathbf{Q} = \begin{pmatrix} \cos(\beta) & \sin(\beta) \\ -\sin(\beta) & \cos(\beta) \end{pmatrix} \tag{1.17}$$

and β the discontinuity angle as shown in fig. 1.3.

In this local frame a cohesive law can be applied to relate the cohesive tractions ($\hat{\mathbf{t}}$) to the displacement jump:

$$\hat{\mathbf{t}}^+ = -\hat{\mathbf{t}}^- = \hat{\mathbf{t}} = \hat{\mathbf{t}}([\![\hat{\mathbf{u}}]\!]) \tag{1.18}$$

The linearized tangent matrix follows as:

$$\hat{\mathbf{T}} = \frac{\partial \hat{\mathbf{t}}}{\partial [\![\hat{\mathbf{u}}]\!]} \tag{1.19}$$

The traction vector and tangent matrix can then be transformed back into the global coordinate system via:

$$\mathbf{Q}^T \hat{\mathbf{t}} = \mathbf{t} \tag{1.20}$$

$$\mathbf{Q}^T \hat{\mathbf{T}} \mathbf{Q} = \mathbf{T} \tag{1.21}$$

The contribution of the two overlapping elements to the internal force vector is given by:

$$\mathbf{f}^{int+} = \int_{\Omega_{e^+}} \mathbf{B}^T \boldsymbol{\sigma}(\boldsymbol{\epsilon})\ \mathrm{d}\Omega_{e^+} + \int_{\Gamma_k} \mathbf{N}^T \mathbf{t}\ \mathrm{d}\Gamma \tag{1.22a}$$

$$\mathbf{f}^{int-} = \int_{\Omega_{e^-}} \mathbf{B}^T \boldsymbol{\sigma}(\boldsymbol{\epsilon})\ \mathrm{d}\Omega_{e^-} - \int_{\Gamma_k} \mathbf{N}^T \mathbf{t}\ \mathrm{d}\Gamma \tag{1.22b}$$

and their contribution to the global stiffness matrix (eq. (1.7)) is given by:

$$\mathbf{K} = \begin{pmatrix} \mathbf{K}^+ & \mathbf{0} \\ \mathbf{0} & \mathbf{K}^- \end{pmatrix} + \begin{pmatrix} \mathbf{K}_{[\![\mathbf{u}]\!]} & -\mathbf{K}_{[\![\mathbf{u}]\!]} \\ -\mathbf{K}_{[\![\mathbf{u}]\!]} & \mathbf{K}_{[\![\mathbf{u}]\!]} \end{pmatrix} \tag{1.23}$$

with

$$\mathbf{K^i} = \int_{\Omega^i} \mathbf{B}^T \mathbf{D} \mathbf{B} \mathrm{d}\Omega^i, \quad i = +, - \tag{1.24}$$

$$\mathbf{K}_{[\![\mathbf{u}]\!]} = \int_{\Gamma_k} \mathbf{N}^T \mathbf{T} \mathbf{N} \mathrm{d}\Gamma_k \tag{1.25}$$

where $\mathbf{D}$ is the elastic tangent matrix $\mathbf{D^e}$.

Chapter 2: Physics of fiber kinking

The phenomenon of fiber kinking has been a subject of interest for many years resulting in numerous publications on various aspects of kinking. The sheer volume of work published on the subject indicates a near impossibility to obtain a complete view of the work conducted on the subject. In this chapter several of the key experimental, numerical and analytical finding are reviewed in order to form a better understanding of the physics of fiber kinking and the important characteristics that must be addressed by the computational model.

2.1. Experimental and numerical observations

Throughout the years various researchers have attempted to gain experimental evidence on the mechanism of fiber kinking [25,32]. This has proven rather challenging due to the unstable nature of failure and the difficulty to observe specimens at a micro-scale during failure. This has led to the use of micro-mechanical finite element models to complement experimental findings [25, 32]. From these studies it has been identified that fiber kinking i.e. kink band formation is mainly a result of fiber misalignment and matrix yielding. Failure by kink band formation can be divided into three phases:

Initiation, in which initially misaligned fibers are subjected to micro-buckling, where, the fibers undergo a rotation α (additional to the initial misalignment angle α_i) within a band. This rotation results in high shear stresses in the matrix causing local yielding and further fiber rotation.

Propagation, where the band grows in transverse direction. Both experimental and numerical studies have shown that kink bands tend to propagate at a certain angle with respect to the normal direction (known as the propagation angle β). This angle is known to evolve as failure progresses through the specimen, however, Sutcliffe and Fleck [30] have shown that kink bands reorient themselves naturally as they propagate to point in a stabilized β direction. The stabilized β angle is usually achieved prior to reaching the limit load.

Broadening, where the band width w grows in axial direction into un-kinked material, the final band width is usually defined when the fibers break under combined bending and compression. Studies [5, 18] have shown that broadening is caused by a "lock up" effect experienced by the matrix, the band then expands under a constant stress (known a broadening stress).

Kink bands are characterized by three parameters: the fiber rotation angle $\alpha + \alpha_i$, the propagation angle β and the band width w (see fig. 2.1).

Waas and Schultheisz have shown in their review [32] several important parameters affecting kink band geometry and composite strength. In general the compressive strength was found to increase with the fiber diameter (improvement on bending stiffness), fiber volume fraction (higher stiffness and strength of fiber compared to matrix) and fiber stiffness (improvement on

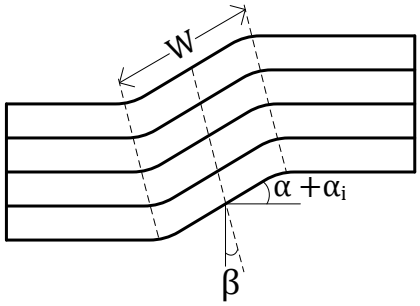

Figure 2.1: Schematic representation of kink band.

bending stiffness). However when fiber diameters and volume fractions become too high, failure is dominated by manufacturing errors. The role of the matrix properties was also assessed, it was found that an increase in matrix strength and stiffness have a significant influence in the overall response of the composite. The interface between matrix and fiber has also been shown to be influential, a weak interface usually leads to failure by splitting, while composites with a strong interface fail by fiber kinking. Pinho et al. have also pointed out in their review [25] that kink bands are sensitive to the specimens stress state. An increase in hydrostatic pressure leads to an increase in failure stress and combining in-plane shear with longitudinal compression significantly reduces the compressive strength. Furthermore Bažant et al. [2] have shown strong size dependencies for the nominal strength of specimens failing purely by kink band propagation. The unstable and (experimentally) uncontrollable nature of fiber kinking has also been discussed by Kyriakides et al. [15], in their experimental and numerical studies, where sharp snap-back behavior was identified for the post-peak response of composites failing by kink band formation.

2.2. Analytical models

Several analytical models can be found in literature to predict the compressive strength associated with kink band formation, these models can be divided into three main categories, micro-buckling theory [26], kinking theory [1] and bending theory [10].

2.2.1. Micro-buckling theories

Micro-buckling theories are based on a micro-mechanical approach in which fiber instability causes failure and were first proposed by Rosen [26]. Rosen hypothesized that failure would occur once the shear mode buckling load was reached and assumed that fibers are perfectly aligned at the start of loading and supported by an elastic matrix. From this hypothesis Rosen derived the well known eq. (2.1).

$$\sigma_c = \frac{G_m}{1 - v_f} \tag{2.1}$$

with G_m and v_f the shear modulus of the matrix and fiber volume fraction respectively. These earlier models severely overestimated the composites compressive stress. Numerous researchers have attempted to improve Rosen's model and some of the later refinements do provide a reasonable estimation for the compressive strength however contain empirical factors [19]. Schultheisz and Waas have presented several arguments against micro-buckling theories in their review [27]. They point out that if fiber kinking is a consequence of micro-buckling one would expect that the kink band boundary would lie in the plane of the highest bending stresses in which case the edges of the kink band should be perpendicular to the loading axis. Fiber micro-buckling is also expected to occur everywhere in the composite at about the same time. Both of these

phenomena are rarely seen experimentally making the case for a separate failure mechanism governing kink band formation.

2.2.2. Kinking theories

Kinking theories are based on the assumption that an initially misaligned fiber causes shear stresses in the surrounding matrix when loaded in compression, once the matrix fails/yields fibers lose their support and fail as a consequence. Argon [1] was the first to consider kinking as a separate failure mechanisms and considered only the initial misalignment in his derivations. Budiansky [3] later improved Argon's model to account for further fiber rotation leading to eq. (2.2).

$$\sigma_c = \frac{\tau_y}{\alpha_i + \gamma_y} \tag{2.2}$$

Where $\alpha_i, \tau_y, \gamma_y$ are the initial fiber misalignment angle, matrix shear yield strength and matrix shear yield strain respectively. These earlier models however were only aimed at predicting the compressive strength of the composites, not the post peak response and did not take multi-axial loading into account. Further developments by Budiansky et al. [4] and Slaughter et al. [28] have included these effects. They considered the traction continuity at the boundary between un-kinked material and kinked material to derive eq. (2.3) under the assumption of in-extensible fibers and small fiber rotation angles $\alpha + \alpha_i$.

$$\sigma^\infty - 2\tau^\infty \tan(\beta) \approx \frac{\tau - \tau^\infty + (\sigma_T - \sigma_T^\infty)\tan(\beta)}{\alpha_i + \alpha} - \sigma_T \tag{2.3}$$

The stresses in eq. (2.3) follow from fig. 2.2.

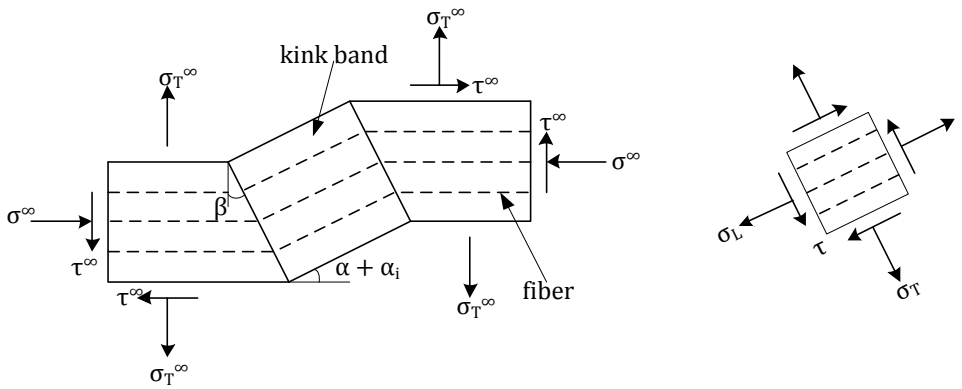

Figure 2.2: Schematic of kink-band, showing sign convention used for derivation of eq. (2.3) in [4, 28].

It is important to note that these earlier models made use of an infinite band assumption i.e. assuming that the kink band was of finite width and infinite length. This assumption implied that all fibers within the band have the same initial misalignment (α_i) and undergo rotation (α) simultaneously at a fixed angle (β). It was later shown by Fleck et al. [11] that this assumption had little consequence when considering only the compressive strength of the composite, with a finite band strength exceeding the infinite band strength by less than 20%[1]. When analyzing propagation of kink bands however the infinite band assumption is no longer valid since for propagation rotation of fibers should not occur simultaneously.

[1]For typical band width value of 20 times the fiber diameter.

2.2.3. Bending theories

Bending theory was first address by Fleck et al. [10] by taking the bending resistance of the fibers into account. Fleck et al. treated the composite as an anisotropic homogeneous solid and used couple stress theory to account for the bending resistance of the fiber. In other works Fleck and Shu [11] have shown that the governing (weak) equations for a fiber-matrix unit cell are identical to those of the Cosserat couple stress theory[2]. Subsequently Fleck et al. [10] derived the relation eq. (2.4), relating the compressive stresses to the additional fiber rotation.

$$\omega(0) = \frac{1}{\Lambda} + C_1 + \frac{\Lambda\omega_i}{\left(\frac{\pi}{2\xi_I}^2 - \Lambda\right)} \tag{2.4}$$

Where ω, Λ and ξ_I are nondimensionalized parameters representing fiber rotation, compressive stress and initial misalignment wavelength, respectively, and C_1 is a constant which is determined by solving for the current deformed shape of the composite.

Other researchers [6, 23] have used micro-mechanical considerations to include bending resistance. These models would explicitly introduce the fiber and matrix and consider bending equilibrium of a single misaligned fiber. The models usually differ in the constitutive relations used for the matrix and the solution procedure used.

Bending theories have ultimately shown that while the fiber bending resistance plays a crucial role in fiber failure and band width, its effect on the pre-failure behavior is negligible and its effect on the post-failure behavior is only evident at large rotations, where in most cases fibers have already failed.

2.2.4. Other theories

Researchers have also considered other approaches to the fiber kinking problem. Dávila et al. [7] developed a model closely resembling kinking theories combining Argon's approach with a matrix failure criterion. The basis of this model is that the stresses occurring in a region of misaligned fibers are rotated to the misaligned coordinate system, the rotated stresses are subsequently used to evaluate the matrix failure criterion to test for failure. The model was further developed and implemented[3] by Pinho et al. [24] and Maimí et al. [16, 17]. In their implementation both Pinho et al. and Maimí et al. used continuum damage theory incorporating energy release rates associated with kinking to approximate the post-peaks behavior of the composite.

Contrary to earlier proposed models Gutkin et al. [13] proposed a model based on a fracture mechanics approach. The model is based on the energy balance of the embedded fiber and the hypothesis that the fiber kinking strength is reached when the strain energy released is equal to the fracture energy.

As knowledge on the fracture process of kink bands increase, more information becomes available on the energy release rates of kink bands improving the accuracy of energy based models. For existing energy models it has been shown that the original formula of Budiansky eq. (2.2) can be recovered when simplified. These energy models have ultimately provided similar solutions to those of kinking and bending theories.

[2]Which they would further develop into a finite element code for the analysis of fiber kinking using Cosserat continuum elements.

[3]Using the finite element method.

2.3. Conclusion

Considering the numerous analytical theories developed, the need for a proper understanding of the physics and mechanics of fiber kinking is even more evident. Recent studies [12, 22] have been able to observe the process of fiber kinking at a micro-scale and have allowed for a better understanding of kink band formation and evolution. It is clear from experimental and numerical studies that fiber kinking is a micro-mechanical process driven by matrix failure due to shear stresses.

An important conclusion that can be reached based on the results of experimental studies is the sequence of events associated with fiber kinking. In particular the initiation and localization of the kink band, where matrix failure/yielding and micro-structural defects such as misaligned fibers and matrix micro-cracks, play an important role. This sensitivity to defects directly implies a statistical dependency explaining the large scatter often seen between experiments. During failure a closed loop is formed between fiber rotation inducing in-plane shear stresses onto the matrix and matrix failing allowing for further fiber rotation. Gutkin et al. [12] showed that this process can also be induced by shear driven fiber compressive failure, however the main characteristics of fiber kinking remain unchanged. Recent authors [2, 13, 25] have also shown the importance of energy release associated with kink bands.

Another important observation that can be made from the studies evaluated in this chapter is the composites behavior under uniaxial compression. The composite exhibits a linear elastic behavior prior to failure and a softening behavior governs the post-failure regime.

The various analytical studies conducted on the topic have presented a number of failure criteria that can be used to predict the kinking failure load with relative accuracy. Whether fiber kinking is addressed via micro-buckling theories, kinking theories or other theories several conclusions can be made based on the the numerous studies conducted on the subject. What follows is a short summary of assumptions concluded from literature that will be used throughout this thesis.

A-1 Upon reaching the failure load fibers have already undergone a certain rotation α_f.
As one expects prior to failure the kink bands begin deforming elastically.

A-2 Kink band width are assumed 20 times the fiber diameter.
Experimental values of kink band width usually lie in the neighborhood 10-20 times fiber diameter [9, 10, 25].

A-3 Fibers within a kink-band are assumed in-extensible. Budiansky and Fleck [4] have studied the effects of fiber extensibility on the critical kinking stress and have found it to be negligible when fibers are much stiffer than matrices. As the stiffness ratio between fiber and matrix decreases the influence of the finite fiber stiffness increases and the assumption of in-extensibility is no longer valid. For common fiber composites, however, this is not the case as fibers are much stiffer then the surrounding matrix material.

Chapter 3: Kink band modeling

The goal of this thesis is to model fiber kinking in composite laminates. However, in the interest of complete failure analysis of composite laminates it is important to consider the models relation to other failure mechanisms. Because composites are known to exhibit various failure mechanisms that can either compete with- or promote one another, complete failure analysis requires that the interaction between failure mechanisms is incorporated. It is therefore indisputable that in order to construct a model that is useful for both kinking and complete failure analysis, considerations regarding interaction between kinking and other failure mechanisms must be taken into account.

The various experimental research has shown that fiber kinking interact with different failure mechanisms. Kinking has been shown to be promoted by shear inducing mechanisms such as shear driven fiber compressive failure [12] and tend to compete with other shear dominated mechanisms such as ply splitting [25]. Furthermore, kinking often leads to other forms of failure such as delamination and fiber failure [22]. Consequently, it is important to define a failure criterion based on the stress state, not predetermined values such as compressive strength and include proper post-failure constitutive behavior to describe the post-failure stress state.

In this chapter the computational model for fiber kinking analysis is outlined and three models are derived for simulation of the kink band behavior in a discrete setting.

3.1. Model outline

Meso-level models for composite laminates model plies as a homogeneous continua with orthotropic properties related to fiber direction. In order to incorporate failure by fiber kinking on a meso-level, a model is needed that can accurately approximate the composite behavior within a homogeneous framework. This presents several challenges as research has shown that kink band formation and propagation are micro mechanical processes affected by micro mechanical properties. For a reliable fiber kinking failure model, 4 key aspects are required to be incorporated:

- A constitutive law governing the composite response prior to failure (pre-failure behaviour)
- A criterion to determine if failure by fiber kinking has occurred (failure criterion)
- A criterion to determine the direction of transverse propagation of the kink band (propagation angle)
- A constitutive law governing the kinked band response after failure initiation (post-failure behavior)

3.1.1. Pre-failure behavior

As pointed out in chapter 2 the response of the composite prior to the failure load is linear elastic. This observation implies that a linear elastic analysis can be used prior to reaching the failure load. The standard finite element (FE) method can therefore be used to solve the equilibrium equations governing the composite prior to failure. Elements can then be investigated for failure by evaluating a failure criterion at integration point level.

One disadvantage to this approach is that the evolving stress state of the kink band prior to reaching the failure load is not taken into account. However prior to failure the evolving stress state does not have much effect on the behavior at a global level, owing to the localized nature of the kink band and the elastic state of the matrix.

Failure criterion For evaluation of failure the following failure criterion will be used:

$$f(\boldsymbol{\sigma}) = \frac{\sigma_{xx}}{\sigma_c} \leq 1 \tag{3.1}$$

Where σ_{xx} is the current axial stress and σ_c is the critical axial stress.

The critical axial stress is derived using kinking theory for multi-axial loading as derived by Slaughter et al. [28]. For brevity the derivations are only outlined here, for the full derivation the reader is referred to [28]. As explained in chapter 2 the failure load corresponds with the onset of matrix failure (or yielding). Noting the stress state of the kink band (see fig. 2.2), failure of the matrix can be evaluated with the stress criterion:

$$f(\boldsymbol{\sigma}) = \left(\frac{\sigma_T}{\sigma_{Ty}}\right)^2 + \left(\frac{\tau}{\tau_y}\right)^2 \leq 1 \tag{3.2}$$

where τ, σ_T are the current transverse and shear stress of the composite and the subscript y refers to the yield (or failure) stress.

Continuity of traction and displacements across the kink band boundary along with eq. (3.2) and infinite band assumption lead to the critical stress for an ideal plastic matrix [28]:

$$\sigma_c = \frac{a\tau_y - \tau - \sigma_T \tan(\beta)}{\alpha_i + \alpha_f} \tag{3.3}$$

with

$$a = \sqrt{1 + \left(\frac{\sigma_{Ty}}{\tau_y}\right)^2 \tan^2(\beta)} \tag{3.4}$$

The (additional) rotation at failure α_f follows from the yield strain:

$$\alpha_f = \frac{\gamma_y}{a} = \frac{\tau_y}{aG} \tag{3.5}$$

with G the elastic shear modulus and α_i the initial fiber misalignment. The initial fiber misalignment angle α_i is a statistical parameter that embodies the micro-structural defects and fabrication errors present within the composite. In this thesis α_i is assumed to be a known material parameter and is taken to be four times the failure rotation α_f[1]. Statistical analysis is needed in order to determine accurate values for α_i.

For the uni-axial stress state as will be considered in this thesis the expression for σ_c can be rewritten to:

$$\sigma_c = \frac{a\tau_y}{\alpha_i + \alpha_f} \tag{3.6}$$

[1]This is in keeping with the typical values for fiber misalignment of $2° - 4°$.

Propagation angle For the propagation angle a fixed angle (β) is assumed. Although experimental and numerical investigations show an evolving propagation angle, post-peak propagation usually occur at a stabilized β direction. The angle is determined using the relation derived by Niu et al. [20].

$$\beta = \arctan(1 - c) \tag{3.7}$$

with c the fiber volume fraction.

3.1.2. Post-failure behavior

When addressing the question of how the post failure behavior can be incorporated in the model two approaches can be considered, a continuous approach or a discontinuous approach. It is clear that at a micro scale only a continuous approach is adequate.

On a meso-level however, considering the localized nature of kink bands a continuous approach would lead to mesh sensitivity. The use of regularization techniques could reduce this sensitivity however since kink bands are relatively small and localized, accurate depiction of kink bands would still require a very fine mesh. Several authors [17,24,29] have used continuum failure models to define kink bands on a meso-level however these models fail to properly localize failure in a finite band width when a coarse mesh is used. Furthermore if one was to assume that the kink band width remains fixed at typical values of 10-20 times the fiber diameter, at a meso-level, the kink bands can be interpreted as strong discontinuities within the continuum and a discontinuous approach is to be preferred.

In the current work the choice is made to approximate kink bands as strong discontinuities. The discontinuity is introduced once the failure criterion eq. (3.1) is violated (see figs. 3.1a and 3.1b).

For post-failure analysis, XFEM is used to introduce the post failure behavior of the new discontinuous element. The kink band constitutive law will be incorporated in a cohesive zone (see fig. 3.1c) via a discrete cohesive law presented in section 3.2, while unkinked (bulk)material remains linear elastic. The phantom node version of XFEM is chosen over the traditional partition of unity methods due to its more simplistic implementation and suitability for cohesive crack modeling as pointed out by van der Meer [31].

In the formulation of the phantom node method presented in section 1.5.2, failure is constituted over the full width of an element and the tip of the kink band will propagate element by element at the fixed propagation angle β defined in eq. (3.7). At *element level* the infinite band assumption used in derivation of the failure criterion fits well within the phantom node framework[2] and will be used in derivation of the cohesive law in section 3.2.

At *system level* the band length is ultimately limited to the width of an element, indicating a finite band. Because failure is constituted over the full width of the element, a mesh dependency will be present when considering failure propagation. However, considering both; the varying displacement jumps at each (cohesive) integration point[3] and the redistribution of stresses, the effects of propagating kink bands can still be simulated.

A final note on the discontinuous approach for kink bands is that a limitation is present when addressing the phenomenon of band broadening. Because the kink band width is not physically incorporated in the model and was assumed fixed, band broadening cannot be physically addressed. Mechanically however it is possible to incorporate aspects of band broadening such as the onset of broadening and the broadening stress in the cohesive law. However, as there are still many developing theories on the occurrence of broadening it is left out of the scope of this thesis.

[2]Since failure is constituted over the full width of the element.

[3]Depending on the number of cohesive integration points per element.

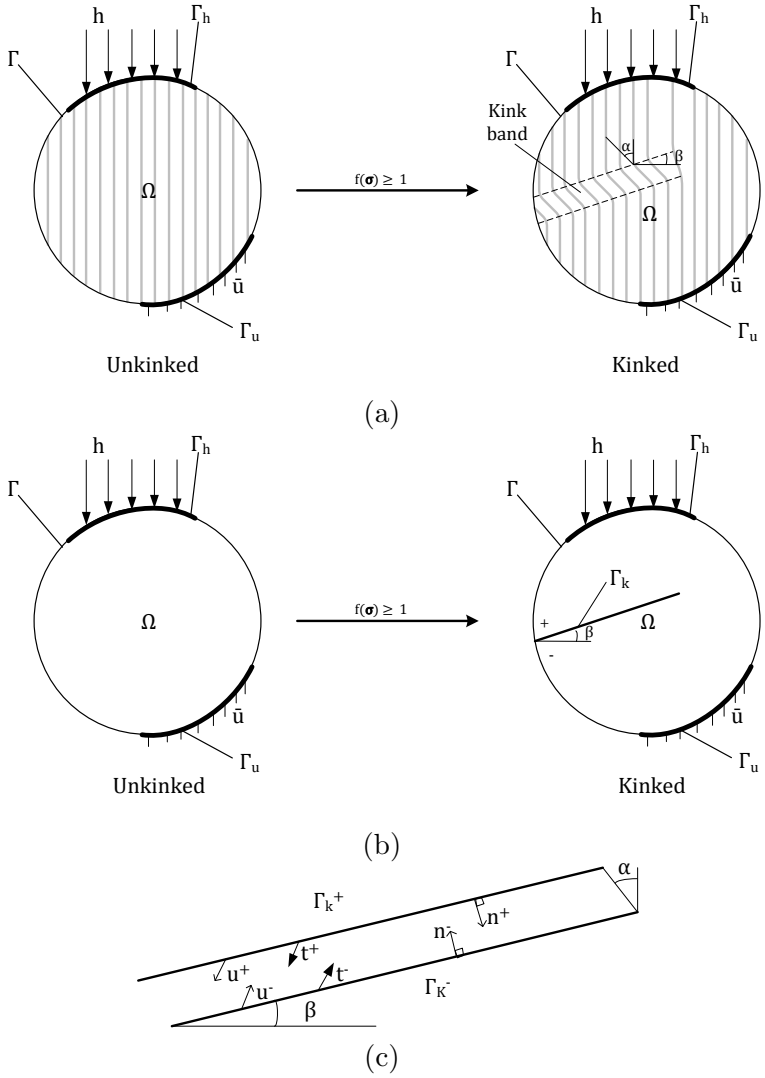

Figure 3.1: (a)Fiber matrix material (b)Homogenized approximation (c)Zoom in of kinked zone.

3.2. Cohesive zone modeling

The proposed failure model presented in section 3.1.2 requires a cohesive relation which incorporates the kink band constitutive behavior in a traction-separation law. Derivation of such a law requires, firstly, description of the mechanics of kink bands and, secondly, translation of these onto a discrete setting. Furthermore, the proposed failure model necessitates an initially rigid law, as discontinuities are introduced at non-zero stress levels.

Here three discrete cohesive models are derived. Starting point for these model is a micro-mechanical description of the kink band, from there three different approaches are used to simulate the collapse of the kink band.

Before proceeding it is important to note that from the description of kink bands, three coordinate frames can be identified (see fig. 3.2), a $\{x, y\}$-frame a $\{n, s\}$-frame and a $\{\epsilon_1, \epsilon_2\}$-frame. Unless otherwise stated the following conventions will be used with regards to the coordinate frames. The $\{x, y\}$-frame is the global coordinate frame with x coinciding with the direction of the fibers. Parameters in the $\{x, y\}$-frame will be denoted with plain symbol. The $\{n, s\}$-frame is the local discontinuity frame (corresponding with propagation angle β) with n the normal to the discontinuity and will be referred to as the β-frame. Parameters in the $\{n, s\}$-frame are denoted with $\hat{\cdot}$. The $\{\epsilon_1, \epsilon_2\}$-frame is the local kink band frame with ϵ_1 the

local fiber direction therefore the $\{\epsilon_1, \epsilon_2\}$-frame rotates along with the fiber. Parameters in the $\{\epsilon_1, \epsilon_2\}$-frame are denoted with $\bar{\cdot}$.

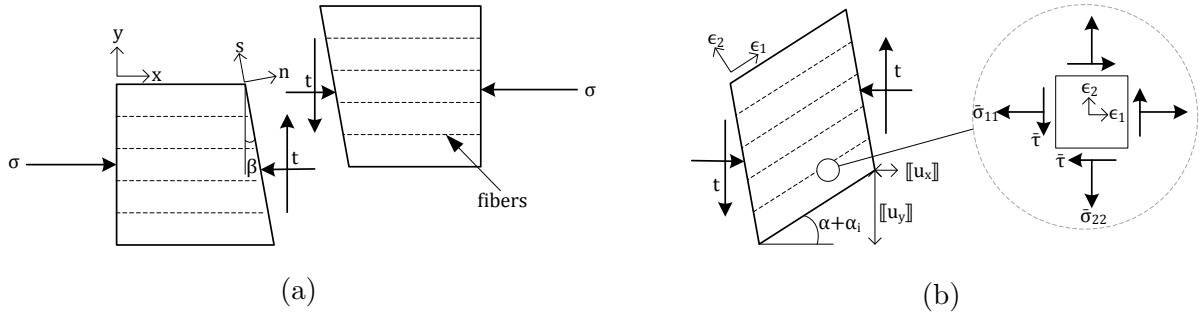

(a) (b)

Figure 3.2: (a) Free body diagram of discontinuous element. (b) Free body diagram of kink band and kink band stresses.

3.2.1. Continuum description

In order to accurately depict the post-peak response of the kink band, a proper description of the continuum stress state is required. During loading, fibers within the band are subjected to a rotation α, leading to the development of strains within the band. Under the assumption of in-extensible fibers and in accordance with [4] the strains can be defined in terms of the fiber rotation as:

$$\bar{\varepsilon}_{11} \approx 0 \tag{3.8a}$$

$$\bar{\varepsilon}_{22} = \ln\left(\frac{\cos(\beta - \alpha - \alpha_i)}{\cos(\beta - \alpha_i)}\right) \approx \alpha \tan(\beta) \quad \text{for} \quad \alpha \ll 1 \tag{3.8b}$$

$$\bar{\gamma} = \alpha \tag{3.8c}$$

Prior to failure, kink bands behave elastically following the common elastic relation leading to development of axial stress $\bar{\sigma}_{11}$, transverse stress $\bar{\sigma}_{22}$ and shear stress $\bar{\tau}$, as indicated in fig. 3.2. The kink band is assumed to be characterized by an elastic stiffness relation given by:

$$\bar{\mathbf{D}} = \begin{pmatrix} E_{11} & 0 & 0 \\ 0 & E_{22} & 0 \\ 0 & 0 & G \end{pmatrix} \tag{3.9}$$

with E the Young's modulus, G the shear modulus of the composite. Since deformation primarily occurs through rotation of the fibers and shearing, lateral contraction does not play a major role and are neglected. In most composites the matrix material is much more compliant than the fibers, while fibers are only active in axial direction. It can therefore be assumed that the matrix caries shear and transverse stresses and the fibers carry axial forces.

As explained in section 3.1.1 failure is constituted once the matrix failure (or yield) criterion is violated. In previous text on kinking theory [3, 4, 28] the matrix was assumed to deform plastically after reaching the yield limit and it is at this point that the choice of ideal or hardening plasticity would play a role. However, the choice for ideal or hardening plasticity may be of little significance when considering the fact that the matrix may undergo micro-cracking. From the definition of the strains it follows that the non-zero $\bar{\varepsilon}_{22}$, together with the assumptions of fiber in-extensibility and plane strain implies that the kinked material undergoes volumetric straining [4]. As pointed out by Budiansky et al. [4], the early stages of kinking may indeed be associated with volume changes attributable to the opening of micro-cracks

in the matrix. Recent experimental evidence (for example [12]) have in-fact shown that the tensile strain $\bar{\varepsilon}_{22}$ and the shear strain $\bar{\gamma}$ do lead to micro-cracking of the matrix which tend to coalesce and form splits between the matrix and fiber. These micro cracks will then result in a reduction in load bearing capacity of the matrix. This reduction can be incorporated by making use of damage mechanics and introducing a damage variable conform eq. (1.13). Since the fibers remain unaffected by the cracking the axial stiffness suffers no reduction and the matrix stresses are given by:

$$\bar{\sigma}_{22} \leftarrow (1-\omega)\bar{\sigma}_{22} \tag{3.10a}$$

$$\bar{\tau} \leftarrow (1-\omega)\bar{\tau} \tag{3.10b}$$

It must be noted that the use of a damage model implies that unloading occurs via a secant branch. Deformation within kink bands however tends to be more of a plastic nature showing little to no elastic recovery.

3.2.2. Model A: Strong discontinuity model

The desired form of the discrete constitutive relation for the kink band can be written in the form:

$$\bar{\mathbf{t}} = \bar{\mathbf{T}}[\![\bar{\mathbf{u}}]\!] \tag{3.11}$$

From the (elastic) continuous description of the kink band the traction at the kink band boundary can be derived following:

$$\bar{\mathbf{t}} = \bar{\mathbf{H}}\bar{\boldsymbol{\sigma}} \tag{3.12}$$

where $\bar{\mathbf{H}}$ is the representation of the normal vector in Voigt notation given by:

$$\bar{\mathbf{H}} = \begin{pmatrix} \cos(\phi-\beta) & 0 & \sin(\phi-\beta) \\ 0 & \sin(\phi-\beta) & \cos(\phi-\beta) \end{pmatrix} \tag{3.13}$$

with $\phi = \alpha + \alpha_i$. Bearing in mind the relation between the stresses and strains, the traction can be written as:

$$\bar{\mathbf{t}} = \bar{\mathbf{H}}\bar{\mathbf{D}}\bar{\boldsymbol{\varepsilon}} \tag{3.14}$$

The strains can be written in terms of the discontinuity by making use of strong discontinuity kinematics, as presented by Oliver [21], such that:

$$\bar{\boldsymbol{\varepsilon}} = \mathbf{R}\boldsymbol{\varepsilon} + \frac{1}{w}\left(\bar{\mathbf{H}}^T[\![\bar{\mathbf{u}}]\!]\right)^s \tag{3.15}$$

with ε the strains outside of the kink band and $\mathbf{R}$ a rotation matrix and w the kink band width. Because deformation is localized in the kink band it can be assumed that $\varepsilon \to 0$. It is worth noting that if eq. (3.15) is pre-multiplied with w and the limit of $w \to 0$ is taken, ε still vanishes. However, here it is preferred to include the kink band width in order to allow for possible extensions to band broadening. Inserting eq. (3.15) into eq. (3.14) then leads to:

$$\bar{\mathbf{t}} = \underbrace{\frac{1}{w}\bar{\mathbf{H}}\bar{\mathbf{D}}\bar{\mathbf{H}}^T}_{\bar{\mathbf{K}}^{\mathbf{e}}}[\![\bar{\mathbf{u}}]\!] \tag{3.16}$$

where $\bar{\mathbf{K}}^{\mathbf{e}}$ is the so-called elastic acoustic tensor. $\bar{\mathbf{K}}^{\mathbf{e}}$ represents the stiffness prior to the onset of kinking when no inelastic deformation has taken place. Before onset of kinking one can find:

$$\bar{\mathbf{K}}^{\mathbf{e}} = \bar{\mathbf{H}}_i\bar{\mathbf{D}}\bar{\mathbf{H}}_i^T \tag{3.17}$$

where $\bar{\mathbf{H}}_i$ is the initial unit normal determined by inserting $\phi = \alpha_i$ into eq. (3.13).

From eq. (3.16) it is immediately apparent that the traction is not well defined upon failure initiation i.e., when $[\![\bar{\mathbf{u}}]\!] = 0$. In order to construct an initially rigid law a shift is introduced such that the traction is computed from a translated displacement jump $[\![\bar{\mathbf{v}}]\!]$:

$$\bar{\mathbf{t}} = \bar{\mathbf{K}}^{\mathbf{e}}[\![\bar{\mathbf{v}}]\!] \tag{3.18}$$

with

$$[\![\bar{\mathbf{v}}]\!] = [\![\bar{\mathbf{u}}]\!] + [\![\bar{\mathbf{u}}]\!]_f \tag{3.19}$$

The shift $[\![\bar{\mathbf{u}}]\!]_f$ is computed from the requirement that for zero opening $\bar{\mathbf{t}} = \mathbf{Q}_f\mathbf{H}\boldsymbol{\sigma}_f$ this gives:

$$[\![\bar{\mathbf{u}}]\!]_f = (\bar{\mathbf{K}}^{\mathbf{e}})^{-1}\mathbf{Q}_f\mathbf{H}\boldsymbol{\sigma}_f \tag{3.20}$$

where the subscript f denotes the stress state at failure and $\mathbf{Q}_f$ is the rotation matrix defined as:

$$\mathbf{Q}_f = \begin{pmatrix} \cos(\phi_f) & \sin(\phi_f) \\ -\sin(\phi_f) & \cos(\phi_f) \end{pmatrix} \tag{3.21}$$

and $\phi_f = \alpha_f + \alpha_i$ and $\mathbf{H}$ given by:

$$\mathbf{H} = \begin{pmatrix} \cos(\beta) & 0 & \sin(\beta) \\ 0 & \sin(\beta) & \cos(\beta) \end{pmatrix} \tag{3.22}$$

Having defined the initial elastic relation, the damageable matrix description must be implemented for the post-peak response. Insertion of eq. (3.10) into eq. (3.12) results in:

$$\bar{t}_1 = \bar{\sigma}_{11}\cos(\phi - \beta) + (1-\omega)\bar{\tau}\sin(\phi - \beta) \tag{3.23a}$$
$$\bar{t}_2 = (1-\omega)(\bar{\sigma}_{22}\sin(\phi - \beta) + \bar{\tau}\cos(\phi - \beta)) \tag{3.23b}$$

Because fiber rotations are assumed to remain small during damage evolution it follows that $\bar{\sigma}_{11} \gg \bar{\tau}$, consequently the influence of $\bar{\sigma}_{11}$ on $\bar{t}_1$ is greater then that of $\bar{\tau}$. Therefore $\bar{t}_1$ is assumed unaffected by the damage variable and eq. (3.23) can be simplified such that:

$$\bar{t}_1 = \bar{t}_1 \tag{3.24a}$$
$$\bar{t}_2 \leftarrow (1-\omega)\bar{t}_2 \tag{3.24b}$$

It must be noted that if t_1 was positive i.e. in tension, energy could then also be dissipated by the rupture of the fiber. In this case t_1 is affected by damage and the assumption of inextensibility may no longer be valid. However in this thesis only compression is considered.

Damage evolution An exponential damage evolution law is used to compute ω. With increasing knowledge of the fracture mechanical aspect of kink bands a more realistic representations for damage evolution may become available. However, for the sake of simplicity exponential softening is assumed.

$$\omega = 1 - \frac{1}{r}\exp(A(1-r)) \tag{3.25}$$

The parameter A is a scaling parameter related to the fracture energy, and r is an internal variable that is equal to 1 when damage is initiated.

It is clear from the continuum description of the kink band that failure is driven by fiber rotation α which is related to the transverse displacement jump $[\![\bar{u}_2]\!]$, consequently the internal variable can be defined as:

$$r = \frac{[\![\bar{v}_2]\!]}{[\![\bar{u}_2]\!]_f} \tag{3.26}$$

Evolution of the internal variable $\dot{r}$ is such that the Kuhn-Tucker conditions are satisfied:

$$f \leq 0,\ \dot{r} \geq 0,\ f\dot{r} = 0 \tag{3.27}$$

where f is the damage activation function.

The scaling parameter A is determined from the energy balance equation given by:

$$G_{\text{kink}} = \int \bar{t}_1 \mathrm{d}[\![\bar{u}_1]\!] + \int \bar{t}_2 \mathrm{d}[\![\bar{u}_2]\!] \tag{3.28}$$

Since $\bar{t}_1$ is assumed not to be associated with energy dissipation the first term of the right hand side of eq. (3.28) can be dropped. Furthermore, as fibers have been assumed in-extensible it follows that the shifted displacement jump in fiber direction remains small. A can now be determined by evaluating eq. (3.28) and making use of $[\![\bar{v}_1]\!] \to 0$.

$$\begin{aligned}
G_{\text{kink}} &= \int \bar{t}_2 \mathrm{d}[\![\bar{u}_2]\!] \\
&= \int_0^\infty (1-\omega)\bar{K}^e_{21}[\![\bar{v}_1]\!] + (1-\omega)\bar{K}^e_{22}[\![\bar{v}_2]\!]\mathrm{d}[\![\bar{u}_2]\!] \\
&= \bar{K}^e_{22}\int_0^\infty \frac{[\![\bar{u}_2]\!]_f}{[\![\bar{v}_2]\!]} \exp(A(1-\frac{[\![\bar{v}_2]\!]}{[\![\bar{u}_2]\!]_f})[\![\bar{v}_2]\!]\mathrm{d}[\![\bar{u}_2]\!] \\
&= \bar{K}^e_{22}[\![\bar{u}_2]\!]_f \int_0^\infty \exp(A - (\frac{A[\![\bar{u}_2]\!]}{[\![\bar{u}_2]\!]_f} + \frac{A[\![\bar{u}_2]\!]_f}{[\![\bar{u}_2]\!]_f}))\mathrm{d}[\![\bar{u}_2]\!] \\
&= \bar{K}^e_{22}[\![\bar{u}_2]\!]_f \int_0^\infty \exp(\frac{-A[\![\bar{u}_2]\!]}{[\![\bar{u}_2]\!]_f})\mathrm{d}[\![\bar{u}_2]\!] \\
&= \frac{\bar{K}^e_{22}[\![\bar{u}_2]\!]^2_f}{A} \to A = \frac{\bar{K}^e_{22}[\![\bar{u}_2]\!]^2_f}{G_{\text{kink}}}
\end{aligned} \tag{3.29}$$

Linearization With the evolution function now defined it follows to determine the linearized tangent in accordance with eq. (1.19) to arrive at the desired form eq. (3.11).

$$\bar{\mathbf{T}} = \frac{\partial \bar{\mathbf{t}}}{\partial [\![\bar{\mathbf{u}}]\!]} = \begin{cases} \bar{T}_{11} &= \frac{\partial \bar{t}_1}{\partial [\![\bar{u}_1]\!]} = \bar{K}^e_{11} \\ \bar{T}_{12} &= \frac{\partial \bar{t}_1}{\partial [\![\bar{u}_2]\!]} = \bar{K}^e_{12} \\ \bar{T}_{21} &= \frac{\partial \bar{t}_2}{\partial [\![\bar{u}_1]\!]} = (1-\omega)\bar{K}^e_{21} \\ \bar{T}_{22} &= \frac{\partial \bar{t}_2}{\partial [\![\bar{u}_2]\!]} = (1-\omega)\bar{K}^e_{22} - \frac{\partial \omega}{\partial r}\frac{\partial r}{\partial [\![\bar{u}_2]\!]}\bar{K}^e_{22}[\![\bar{v}_2]\!] \end{cases} \tag{3.30}$$

with

$$\frac{\partial \omega}{\partial r} = \frac{\exp(A(1-r))}{r^2} + \frac{A\exp(A(1-r))}{r} \tag{3.31a}$$

$$\frac{\partial r}{\partial [\![\bar{u}_2]\!]} = \begin{cases} \frac{1}{[\![\bar{u}_2]\!]_f} & \text{for} \quad f \geq 0 \\ 0 & \text{otherwise} \end{cases} \tag{3.31b}$$

Rotation to global frame The displacement jump and traction have now been defined in the local kink band frame, it now follows to define their relation to the global displacement jump and traction. Both local quantities (displacement jump and traction) are related to their global counterparts through rotation given by:

$$[\![\bar{\mathbf{u}}]\!] = \mathbf{Q}[\![\mathbf{u}]\!] \tag{3.32}$$

$$\mathbf{t} = \mathbf{Q}^T\bar{\mathbf{t}} \tag{3.33}$$

where

$$\mathbf{Q} = \begin{pmatrix} \cos(\phi) & \sin(\phi) \\ -\sin(\phi) & \cos(\phi) \end{pmatrix} \tag{3.34}$$

with $\phi = \alpha + \phi_f$. α is the additional fiber rotation and is determined using an algorithm presented in section 4.1.2.

The global tangent is now given by:

$$\mathbf{T} = \mathbf{Q}^T \bar{\mathbf{T}} \mathbf{Q} \tag{3.35}$$

3.2.3. Model B: Kinking fiber model

Instead of starting from a continuum description of the kink band, one could also start from a discrete model of a kinking fiber. The failing fiber can be seen as an elastically supported bar undergoing buckling with the matrix material represented by a fixed spring (see fig. 3.3a). Keeping in mind that the matrix is damageable since it will undergo cracking during failure, the spring is also damageable. As opposed to the previous cohesive model this model allows

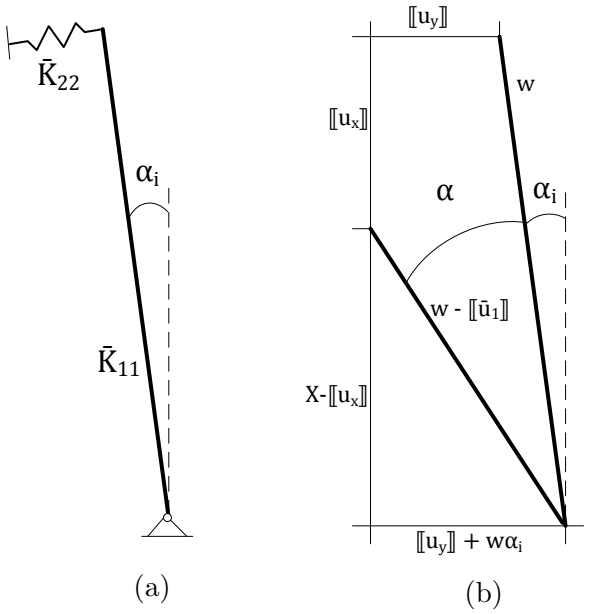

Figure 3.3: (a) Discrete kinking fiber model. (b) Schematic representation of fiber shortening.

for definition of $[\![\bar{\mathbf{u}}]\!]$ in terms of its physical components, $[\![\bar{u}_1]\!]$ is now the fiber shortening and $[\![\bar{u}_2]\!]$ is the compression of the spring and $[\![\bar{\mathbf{u}}]\!] = \mathbf{Q}[\![\mathbf{u}]\!]$ is no longer valid. The definition of $[\![\bar{\mathbf{u}}]\!]$ now follows from geometrical analysis of fig. 3.3b.
Using Pythagoras theorem along with the assumptions; $\alpha_i \ll 1$, $\alpha_i^2 \to 0$, $X \approx w$ and $[\![\bar{u}_1]\!]^2 \to 0$ an expression for $[\![\bar{u}_1]\!]$ can be derived as:

$$(w + [\![\bar{u}_1]\!])^2 = (X + [\![u_x]\!])^2 + ([\![u_y]\!] + w\alpha_i)^2 \tag{3.36a}$$

$$w^2 + [\![\bar{u}_1]\!]^2 + 2w[\![\bar{u}_1]\!] = X^2 + [\![u_x]\!]^2 + 2X[\![u_x]\!] + [\![u_y]\!]^2 + (w\alpha_i)^2 + 2w\alpha_i[\![u_y]\!] \tag{3.36b}$$

$$[\![\bar{u}_1]\!] = [\![u_x]\!] + [\![u_y]\!]\alpha_i + \frac{1}{2w}\left([\![u_x]\!]^2 + [\![u_y]\!]^2\right) \tag{3.36c}$$

During failure the fiber angle increases while the spring remains fixed, $[\![\bar{u}_2]\!]$ therefore follows as:

$$[\![\bar{u}_2]\!] = \mathbf{q}^T [\![\mathbf{u}]\!] \tag{3.37}$$

with $\mathbf{q}^T = \begin{pmatrix} -\sin(\alpha_i) & \cos(\alpha_i) \end{pmatrix}$.

The traction is now defined as the reaction force of the fiber and the spring and therefore in the elastic case the relation $\bar{\mathbf{t}} = \bar{\mathbf{K}}[\![\bar{\mathbf{u}}]\!]$ holds, with $\bar{\mathbf{K}}$ given by:

$$\bar{\mathbf{K}} = \begin{pmatrix} \bar{K}_{11} & 0 \\ 0 & \bar{K}_{22} \end{pmatrix} \tag{3.38}$$

It is clear that since in-extensibility is to be enforced the axial stiffness $\bar{K}_{11} = \frac{E^f}{w} \to \infty$. $\bar{K}_{22}$ must be determined by the matrix resistance, which is far from trivial since the matrix undergoes both shearing and transverse strain. More information is however available on the elastic reaction of the matrix as the rotation angle α_f is known along with the traction at failure $\bar{\mathbf{t}}^f = \mathbf{QH}\boldsymbol{\sigma}_f$. The initial jump $[\![\bar{u}_2]\!]_f$ can be computed noting the relation $[\![\bar{u}_2]\!]_f = w\alpha_f$ and the equivalent stiffness K_{22} is derived as:

$$\bar{K}_{22} = \frac{\bar{t}_2^f}{[\![\bar{u}_2]\!]_f} \tag{3.39}$$

To achieve the initial rigidity required for the cohesive law, again a shift is applied conform eq. (3.19).

Because of the damaging matrix a damage variable is introduced to the spring stiffness and the traction components can be calculated using eq. (3.24). The same exponential damage law as proposed earlier is used. As it still holds that $[\![\bar{u}_1]\!] \to 0$ the damage scaling parameter A remains unchanged. Linearization of the stiffness matrix still follows eq. (3.30) with tangent components $\bar{T}_{11}, \bar{T}_{22}$ unchanged and the off-diagonal terms $\bar{T}_{12} = \bar{T}_{21} = 0$.

Global tangent One issue that deserves special attention when applying this law is the rotation back to the global coordinate frame. Since the reaction force of the spring and fiber do not occur in the same frame a special rotation matrix must be applied such that:

$$\mathbf{t} = \mathbf{Q}_{\text{non}}\bar{\mathbf{t}} \tag{3.40}$$

with $\mathbf{Q}_{\text{non}}$ a non symmetric rotation matrix defined as:

$$\mathbf{Q}_{\text{non}} = \begin{pmatrix} \cos(\phi) & -\sin(\alpha_i) \\ \sin(\phi) & \cos(\alpha_i) \end{pmatrix} \tag{3.41}$$

Furthermore, the linearized tangent in global frame must also be re-derived since $[\![\bar{\mathbf{u}}]\!] \neq \mathbf{Q}[\![\mathbf{u}]\!]$. In this respect the global tangent follows from eq. (1.19) as:

$$\mathbf{T} = \mathbf{Q}_{\text{non}}\bar{\mathbf{T}}\frac{\partial[\![\bar{\mathbf{u}}]\!]}{\partial[\![\mathbf{u}]\!]} \tag{3.42}$$

with

$$\frac{\partial[\![\bar{\mathbf{u}}]\!]}{\partial[\![\mathbf{u}]\!]} = \begin{pmatrix} 1 + \frac{[\![u_x]\!]}{w} & \phi_f + \frac{[\![u_y]\!]}{w} \\ -\sin(\alpha_i) & \cos(\alpha_i) \end{pmatrix} \tag{3.43}$$

3.2.4. Model C: Simplified model

The models previously derived both require determination of the fiber rotation angle α to determine the current $\{\epsilon_1, \epsilon_2\}$-frame. Ultimately as the matrix stiffness decreases the rotation become larger and larger up to the point where the rotations can no longer be assumed small. Since α is also a function of the displacements an additional non-linearity is introduced into the system and $\mathbf{Q}$ is now a function of α and subsequently of $[\![\mathbf{u}]\!]$. Consistent linearization of the tangent would then imply that $\mathbf{T} \neq \mathbf{Q}^T\bar{\mathbf{T}}\mathbf{Q}$. As will be shown in chapter 4 convergence of

these two models become problematic as the analysis progresses and is ultimately terminated prematurely. It would therefore be beneficial if the cohesive model was defined such that the cohesive frame remained fixed.

Sutcliffe and Fleck [30] have shown that kinked material can be modeled, with relative accuracy, as a (mode II) sliding cracks resisted by a shear traction. Sliding then occurs along the fixed angle β.

By ignoring the normal displacements due to rotation it is possible to define a cohesive law in the $\{n, s\}$-frame where the fracture energy is dissipated trough the sliding of the crack faces and interpenetration in normal direction is resisted. This assumption of no normal displacement should not greatly effect the accuracy as analysis of kink bands at micro-level show the displacements in normal direction to be relatively small.
Here a simplified damage law is presented, where again a shifted displacement jump is used to achieve the initial rigidity and account for the initial rotation of the kink band.

Starting from the damage formulation:

$$\hat{\mathbf{t}} = (1-\omega)\hat{\mathbf{K}}[\![\hat{\mathbf{u}}]\!] \tag{3.44}$$

the law is modified such that the traction are computed from the shifted displacements.

$$\hat{\mathbf{t}} = (1-\omega)\hat{\mathbf{K}}[\![\hat{\mathbf{v}}]\!] \tag{3.45}$$

with

$$[\![\hat{\mathbf{v}}]\!] = [\![\hat{\mathbf{u}}]\!] + [\![\hat{\mathbf{u}}]\!]_f \tag{3.46}$$

the subscript f relates to failure initiation. The matrix $\hat{\mathbf{K}}$ in this case represents the equivalent stiffness in $\{n, s\}$ direction with the off-diagonal entries equal to zero. Because interpenetration in normal direction is not permitted it follows again that $\hat{K}_{11} \to \infty$ and $[\![\hat{\mathbf{u}}_n]\!]_f \to 0$. $\hat{K}_{22}$ follows then from:

$$\hat{K}_{22} = \frac{\hat{t}_s^f}{[\![\hat{u}_s]\!]_f} \tag{3.47}$$

where $\hat{\mathbf{t}}^f = \mathbf{Q}_\beta \mathbf{H} \boldsymbol{\sigma}_f$ with

$$\mathbf{Q}_\beta = \begin{pmatrix} \cos(\beta) & \sin(\beta) \\ -\sin(\beta) & \cos(\beta) \end{pmatrix} \tag{3.48}$$

and $[\![\hat{u}_s]\!]_f = [\![\bar{u}_2]\!]_f \cos(\phi_f - \beta)$.

Because of the restriction on the opening in normal direction the damage variable is replaced by a damage tensor. The cohesive law is then rewritten as:

$$\mathbf{t} = (\mathbf{I} - \boldsymbol{\Omega})\hat{\mathbf{K}}[\![\hat{\mathbf{v}}]\!] \tag{3.49}$$

with

$$\boldsymbol{\Omega} = \omega \begin{pmatrix} \frac{\langle \hat{t}_n^{eff} \rangle}{\hat{t}_n^{eff}} & 0 \\ 0 & 1 \end{pmatrix} \tag{3.50}$$

where $\langle \cdot \rangle$ are the Macauley brackets defined as $\langle x \rangle = \max\{0, x\}$ and $\hat{\mathbf{t}}^{eff}$ is the effective traction:

$$\hat{\mathbf{t}}^{eff} = \hat{\mathbf{K}}[\![\hat{\mathbf{v}}]\!] \tag{3.51}$$

Damage evolution still follows the law presented in eq. (3.25). Furthermore, since the jumps in normal direction tend to zero[4], energy balance leads to a similar scaling parameter:

$$A = \frac{\hat{K}_{22}[\![\hat{u}_s]\!]_f^2}{G_{\text{kink}}} \tag{3.52}$$

[4]Since only compression is considered.

The linearized tangent now follows as:

$$\hat{T}_{11} = (1 - \omega \frac{\langle \hat{t}_n^{eff} \rangle}{\hat{t}_n^{eff}}) \hat{K}_{11} \tag{3.53a}$$

$$\hat{T}_{12} = 0 \tag{3.53b}$$

$$\hat{T}_{21} = 0 \tag{3.53c}$$

$$\hat{T}_{22} = (1 - \omega) \hat{K}_{22} - \frac{\partial \omega}{\partial r} \frac{\partial r}{\partial [\![\hat{u}_s]\!]} \hat{K}_{22} [\![\hat{v}_s]\!] \tag{3.53d}$$

with $\frac{\partial \omega}{\partial r}$ and $\frac{\partial r}{\partial [\![\hat{u}_s]\!]}$ determined by replacing $\bar{u}_2$ with $\hat{u}_s$ in eq. (3.31).

Chapter 4: Verification

In this chapter the numerical implementation of the model presented in chapter 3 is discussed. A solution strategy is presented along with several algorithmic aspects. The three cohesive models presented in section 3.2 are applied and their collapse response is evaluated and compared. For clarity, the following convention is used to differentiate between the cohesive models.

- **Model A**: Strong discontinuity model (section 3.2.2)
- **Model B**: Kinking model (section 3.2.3)
- **Model C**: Simplified model (section 3.2.4)

The models are compared to the analytical solution of kinking theory [3] in order to verify the models. Furthermore the sensitivity of the results with respect to different material parameters, known to influence kink bands, is evaluated.

4.1. Numerical Implementation

The model presented in the previous sections is implemented in a one dimensional framework using 2-noded extensible Timoshenko beam elements. Beam elements are used in order to be capable of transmitting the transverse forces introduced by the cohesive law. The choice for the Timoshenko element is due to its simplistic implementation and use of C^0 continuous shape functions.

Extensible Timoshenko beam elements posses three; degrees of freedom, strain quantities and stress-like quantities defined by eq. (4.1).

$$\mathbf{u} = (u_x, u_y, \theta)^T \tag{4.1a}$$

$$\boldsymbol{\varepsilon} = (\varepsilon_{xx}, \gamma, \kappa)^T \tag{4.1b}$$

$$\boldsymbol{\sigma} = (N, V, M)^T \tag{4.1c}$$

Standard linear shape functions are used, as defined in eq. (4.2), in order to interpolate the displacement field in accordance with eq. (1.2).

$$N_1 = \frac{-\xi}{2} + 0.5 \tag{4.2a}$$

$$N_2 = \frac{\xi}{2} + 0.5 \tag{4.2b}$$

with $-1 \leq \xi \leq 1$ With the definition of the **N**-matrix the strains are again related to the displacements in the common fashion as outlined in eq. (1.3) with **L**:

$$\mathbf{L} = \begin{pmatrix} \frac{\partial}{\partial x} & 0 & 0 \\ 0 & \frac{\partial}{\partial x} & -1 \\ 0 & 0 & \frac{\partial}{\partial x} \end{pmatrix} \tag{4.3}$$

For pre-failure behavior and post-failure bulk stress the standard elastic relation exists between the stresses and strains with the $\mathbf{D^e}$-matrix defined as:

$$\mathbf{D^e} = \begin{pmatrix} EA & 0 & 0 \\ 0 & GA_s & 0 \\ 0 & 0 & EI \end{pmatrix} \tag{4.4}$$

Because Timoshenko elements allow bending and shear deformation resulting in transverse (u_y) displacements, the choice of the stiffness GA_s, EI will have implications for the transverse displacement jump $[\![u_y]\!]$ and therefore the cohesive traction. The choice for the shear and bending stiffness should be such that the influence of shear and bending deformation on the displacement jump $[\![u_y]\!]$ remains limited. Furthermore, due to introduction of a rotation degree of freedom (θ) the displacement jump $[\![\mathbf{u}]\!]$ and traction vector $\mathbf{t}$ are extended by $[\![u_\theta]\!], t_\theta$ respectively. However since bending deformation will be limited $[\![u_\theta]\!] \to 0, t_\theta \to 0$. The rotation matrix is also redefined as:

$$\mathbf{Q} = \begin{pmatrix} \cos(\cdot) & \sin(\cdot) & 0 \\ -\sin(\cdot) & \cos(\cdot) & 0 \\ 0 & 0 & 1 \end{pmatrix} \tag{4.5}$$

As mentioned the purpose of this one dimensional study is the evaluation of the post-peak behavior of the model. The use of the phantom node method for post failure modeling implies that failure is localized in a single element. Furthermore owing to the fact that the bulk material stiffness remains elastic and in a one dimensional setting propagation is of no concern only one element is needed to validate the post-peak behavior. Therefore the mesh is drawn up using one element with boundary conditions as indicated in fig. 4.1a.

Pre-failure, numeric integration is carried out using a 1-point Gauss rule. After violation of the failure criteria a cohesive segment is inserted at the location of the *failed* integration point. Post-failure, a new integration scheme is applied, cohesive integration is now located at the previous integration point[1] and integration scheme for the two partially active elements follow 2-point Gauss rule with integration only over the active part as indicated in fig. 4.1c.

4.1.1. Solution procedure

With the constitutive model and the numerical framework introduced a crucial factor in successful failure analysis becomes the introduction of a solution procedure that can ensure convergence of the system without high computational cost. An solution algorithm is presented here based on the solution algorithm formulated by van der Meer et al. for cohesive crack modeling in laminates [31]. An overall summary of the steps is presented in fig. 4.2, in the subsequent sections several components of the procedure are discussed in greater detail.

The core of the solution procedure is the iterative Newton-Raphson (NR) scheme as stated in section 1.4. When a new increment is applied the NR scheme is used until a solution is found that satisfies the convergence criteria. The converged solution is then evaluated at integration point level to check for failure in all elements where failure is permitted. If failure is detected a new kinked segment is inserted or an existing kink band is extended depending on the location of failure, the failure data is then updated and re-inserted into the NR loop. This is done in order to ensure convergence to be possible in subsequent time step [31]. After re-entering the NR loop a solution satisfying the convergence criteria is sought. When propagation is allowed this process is repeated until an equilibrium solution is obtained which does not violate the failure criterion in any location where failure is allowed. A new increment can then be added and the process is restarted.

[1] This is the location of the discontinuity

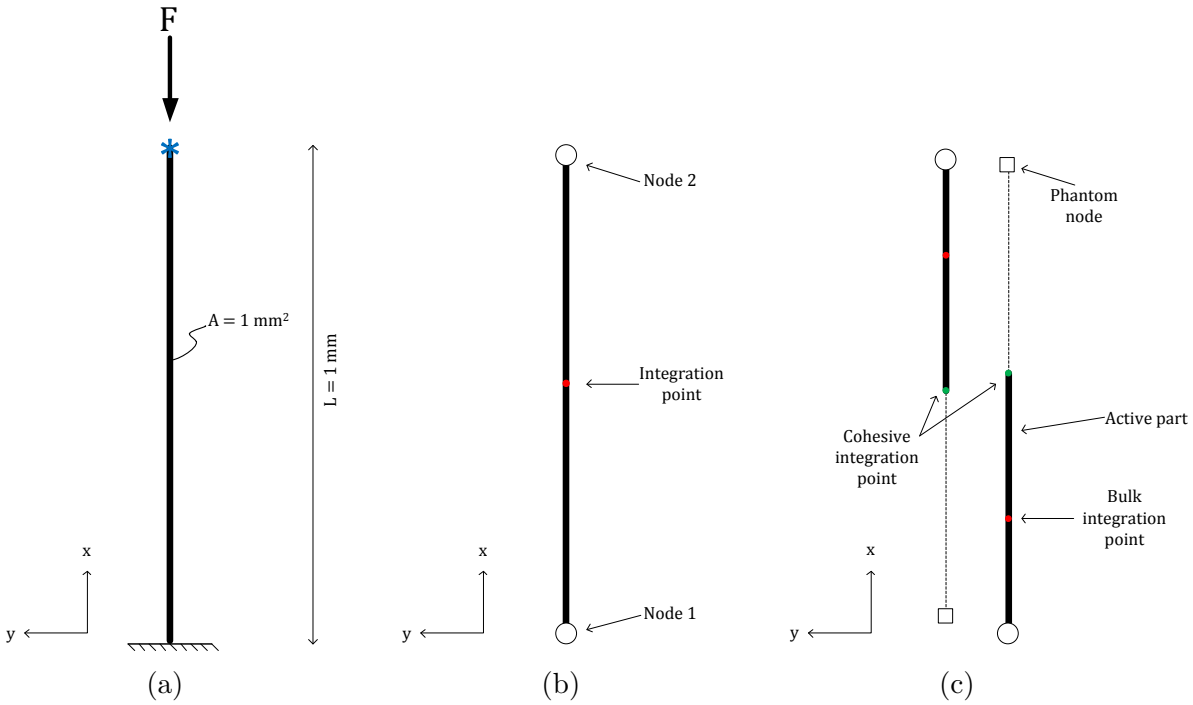

Figure 4.1: (a) Geometry and boundary conditions 1D analysis, note the blue * indicates only rotation constraind. (b) Element, pre-failure. (c) Element, post-failure.

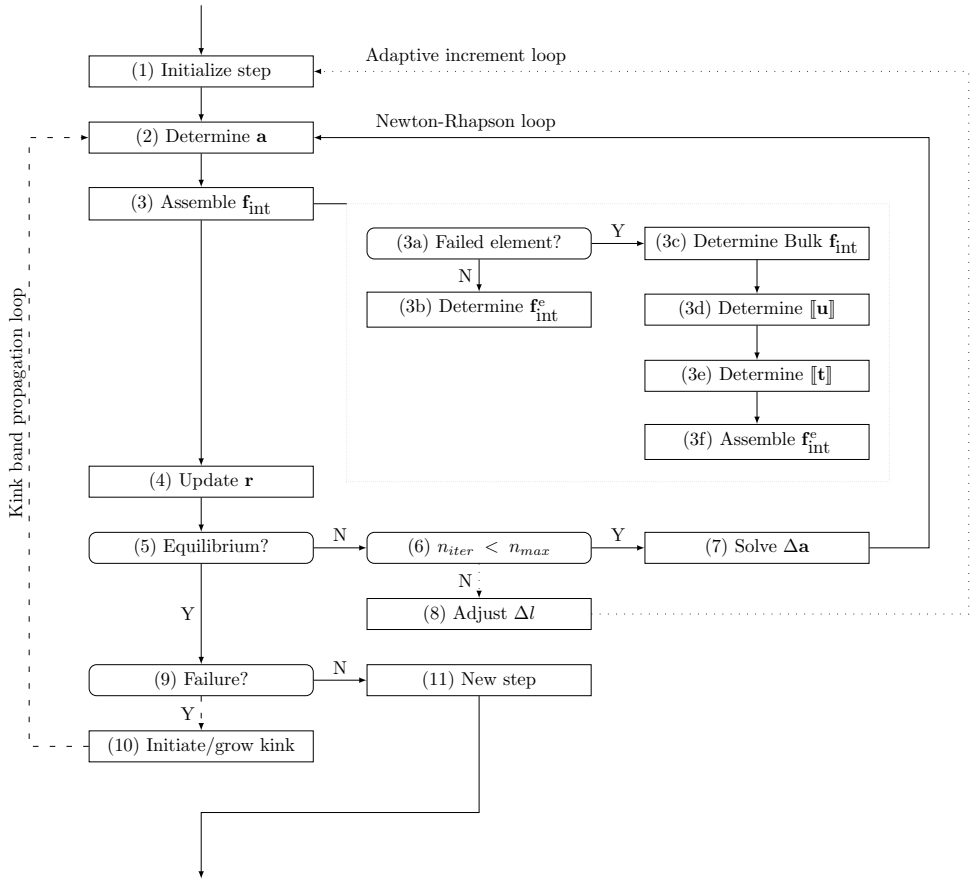

Figure 4.2: Schematized solution procedure.

4.1.2. Local kink band frame

Between steps (3d)-(3e) the cohesive law of models A and B are applied in the local kink band frame. For application of this law it is necessary to first determine the current kink band

frame. In the current iteration the kink band frame is at an angle ϕ^{j+1} with the global frame. Using the kinking theory description of the kink band a relation can be derived between the current frame and the incremental displacement jump $\mathrm{d}[\![\tilde{u}_2]\!]^{j+1}$ (see fig. 4.3). Note that $\mathrm{d}[\![\tilde{u}_2]\!]^{j+1}$ is the incremental jump in the kink band frame of the previous iteration, with angle ϕ^j.

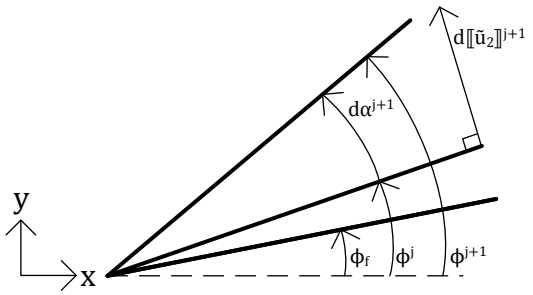

Figure 4.3: One dimensional representation of kink band undergoing rotation.

Beginning from the displacement jump $[\![\mathbf{u}]\!]^{j+1}$ the incremental jump is determined by:

$$\mathrm{d}[\![\mathbf{u}]\!]^{j+1} = [\![\mathbf{u}]\!]^{j+1} - [\![\mathbf{u}]\!]^{j} \tag{4.6}$$

The increment is then rotated to the previous frame ϕ^j:

$$\mathrm{d}[\![\tilde{\mathbf{u}}]\!]^{j+1} = \mathbf{Q}^j \mathrm{d}[\![\mathbf{u}]\!]^{j+1} \tag{4.7}$$

with $\mathbf{Q}^j$ the rotation matrix of the previous iteration. Making use of the in-extensible fiber assumption the incremental rotation angle follows as:

$$\tan(\mathrm{d}\alpha^{j+1}) = \frac{\mathrm{d}[\![\tilde{u}_2]\!]}{w} \rightarrow \mathrm{d}\alpha^{j+1} \approx \frac{\mathrm{d}[\![\tilde{u}_2]\!]}{w} \tag{4.8}$$

which is linearized assuming $\mathrm{d}\alpha \ll 1$. The current frame now simply follows by addition of the increment:

$$\phi^{j+1} = \phi^j + \mathrm{d}\alpha^{j+1} \tag{4.9}$$

4.1.3. Arclength method

As indicated in chapter 2 the unstable nature of kink bands is characterized by a sharp snap-back behavior often seen in the collapse response [15]. This behavior can not be accurately captured by use of a monotonically increasing prescribed displacement at the loaded boundary, for this reason an arclength method is employed to follow the true equilibrium path. In the arclength method the load increment is an additional unknown and the external load vector is defined as:

$$\mathbf{f}_{\mathrm{ext}}^{\mathrm{t}+\Delta\mathrm{t}} = \mathbf{f}_{\mathrm{ext}}^{\mathrm{t}} + \Delta\lambda \check{\mathbf{f}}_{\mathrm{ext}} \tag{4.10}$$

with $\mathbf{f}_{\mathrm{ext}}^{\mathrm{t}}$ the external force of the previous time step, $\Delta\lambda$ the unknown load increment factor and $\check{\mathbf{f}}_{\mathrm{ext}}$ a unit load. The load increment factor is determined by solving an additional constraint equation:

$$\Delta\mathbf{a}_1^T \Delta\mathbf{a}_{j+1} = \Delta l^2 \tag{4.11}$$

where Δl is the length of the equilibrium path (arclength) and $\Delta\mathbf{a}_j$ the global incremental displacement vector in iteration j.

Although the standard arclength has proven to be fairly successful, it has been reported to fail in cases where physical nonlinearities are involved. This is due to the fact that in such cases deformations tend to localize in narrow bands and the global constraint equation eq. (4.11) becomes less meaningful. In the current study failure is highly localized due to the presence

of the discontinuity, the standard arclength method is therefore not suitable for use with the model. A better alternative is the use of indirect displacement methods derived by de Borst [8]. Essentially the difference between indirect displacement methods and standard arclength is that the constraint equation now only contains a limited number of nodal displacement values associated with the location of failure. These nodal quantities are then indirectly controlled, hence indirect displacement control. The major disadvantage of the indirect displacement method is that it is problem dependent, requiring knowledge of the relevant nodes a priori. In combination with XFEM this disadvantage is however of no consequence as the relevant nodes follow directly from the failure data. For the model under consideration the relevant nodes are essentially the phantom nodes that are introduced upon failure initiation.

The Crack Opening Displacement (COD) variant of the indirect displacement method is chosen to track the true equilibrium path, for the COD the constraint equation reads:

$$\delta a_n - \delta a_m = \Delta l \tag{4.12}$$

where δa are incremental displacement of opposing nodes crossed by failure. An advantage of using eq. (4.12) for the constraint equation instead of eq. (4.11) is that the direction of the discontinuity growth can be controlled. Although in most cases one would want that the growth direction follows directly from the constitutive modeling at times it may be advantageous to enforce a particular direction as is the case now. In the one dimensional setting the limit point of the model was found to correspond with a bifurcation point. Two equilibrium states become possible, where the load either increases or decreases. It was found that in cases where growth was in the negative transverse direction an equilibrium state with increasing load was achieved[2]. The opposite response was found when growth was in the positive transverse direction. When the standard constraint equation eq. (4.11) was used, in most cases the increasing path was followed instead of the true decreasing equilibrium path. For this reason the constraint equation eq. (4.12) is used to control the transverse displacement of the phantom nodes.

It is important to note that this directional dependency occurs due to the omission of failure propagation. In two or three dimensional analysis where propagation is included the direction of crack growth is enforced by the inserted propagation angle and the accompanying stress redistribution. In these cases as well as when other failure mechanisms are included, other local or dissipation based arc-length methods would be more suitable.

4.1.4. Loading strategy

When addressing the issues load/displacement increments it is important to take into account its effect on the efficiency and robustness of the computation. While in this thesis computation time is not a major issue due to the use of a single element. Considerations regarding the step sizes are still necessary to insure the simulation is not terminated prematurely.

The failure model outlined in section 3.1 makes use of an elastic constitutive relation pre-failure. It is most efficient to apply an initial load step that is equal to the failure load σ_c in order to pass the elastic branch in one time step. Because a one dimensional analysis is employed with uniaxial condition, σ_c becomes completely deterministic (see eq. (3.6)) and is applied as the initial load step. Following application of the initial load, failure ensues and the arclength method must be employed to capture the post-peak response. For subsequent time steps it is efficient to allow for a varying value of Δl. In this spirit of efficiency the arclength for each time step is determined following the heuristic procedure given by:

$$\Delta l^{\mathrm{t}+\Delta\mathrm{t}} = \Delta l^{\mathrm{t}} \left(\frac{n^{\mathrm{opt}}}{n^{\mathrm{t}}} \right)^{\gamma} \tag{4.13}$$

[2]Due to negative (compressive) traction $\bar{t}_2$

with n^{opt} the optimum number of iterations, n^{t} the number of iterations in the previous time step and γ a weight factor. In order to avoid a lengthy number of iterations a maximum number of iterations $n^{\max}$ is defined, in the case of no convergence an adaptive scheme is employed where the arclength is subsequently reduced using eq. (4.13). When using an adaptive loading scheme it is useful to define limits to the step size such that too large or impractically small increments are avoided.

$$\Delta l_{\min} \leq \Delta l^{\text{t}+\Delta\text{t}} \leq \Delta l_{\max} \tag{4.14}$$

For kinking analysis a good choice for $\Delta l_{\max}$ would be the elastic displacement at failure $[\![\bar{u}_2]\!]_f$ and to set $\Delta l_{\min} = 10^{-3} \cdot \Delta l_{\max}$.

A final note on the arclength is that although an adaptive scheme has been devised due to the initial loading up to failure it is still necessary to define an initial arclength Δl_i to handle the initial time step post-failure. Unfortunately, to the best of the authors knowledge no well founded method for proper choice of the arclength currently exists, however, a sufficiently small value should be chosen in order to ensure convergence. Therefore the choice is made to set $\Delta l_i = \Delta l_{\min}$.

4.2. Collapse response

For the analysis material properties of carbon-epoxy T300/1034-C composite are used, obtained from [17]. The fracture energy associated with kinking was obtained from compact compression test done by Pinho [24] for a carbon composite of the same fiber type (T300/913). A summary of the material and numerical parameters used in the analysis is given in table 4.1.

Table 4.1: Material and Numerical parameters used in analysis.

Composite properties			
Axial stiffness	EA	$146.8 \cdot 10^3$	N
Shear stiffness	GA_s	10^{10}	N
Bending stiffness	EI	10^{10}	Nmm^2
Kink band properties			
Fiber volume fraction	c	0.6	
Fiber diameter	d^f	$7 \cdot 10^{-3}$	mm
Axial young's modulus	E_{11}	10^{10}	N/mm^2
Transverse young's modulus	E_{22}	$11.4 \cdot 10^3$	N/mm^2
Shear modulus	G	$6.1 \cdot 10^3$	N/mm^2
Shear yield stress	τ_y	58.7	N/mm^2
Propagation angle	β	0.381	rad
Kink band width	w	0.14	mm
Initial fiber angle	α_i	$3.38 \cdot 10^{-2}$	rad
Fiber rotation at failure	α_f	$8.4 \cdot 10^{-3}$	rad
Failure stress	σ_c	$1.59 \cdot 10^3$	N/mm^2
Fracture energy	G_{kink}	78.27	N/mm
Numerical parameters			
Optimal number of iterations	n_{opt}	6	
Maximum number of iterations	$n_{\max}$	20	
Weight factor	γ	0.5	
Convergence criterion	$\epsilon_{\min}$	10^{-3}	
Maximum arclength	$\Delta l_{\max}$	$1.18 \cdot 10^{-3}$	mm
Minimum arclength	$\Delta l_{\min}$	$1.18 \cdot 10^{-6}$	mm

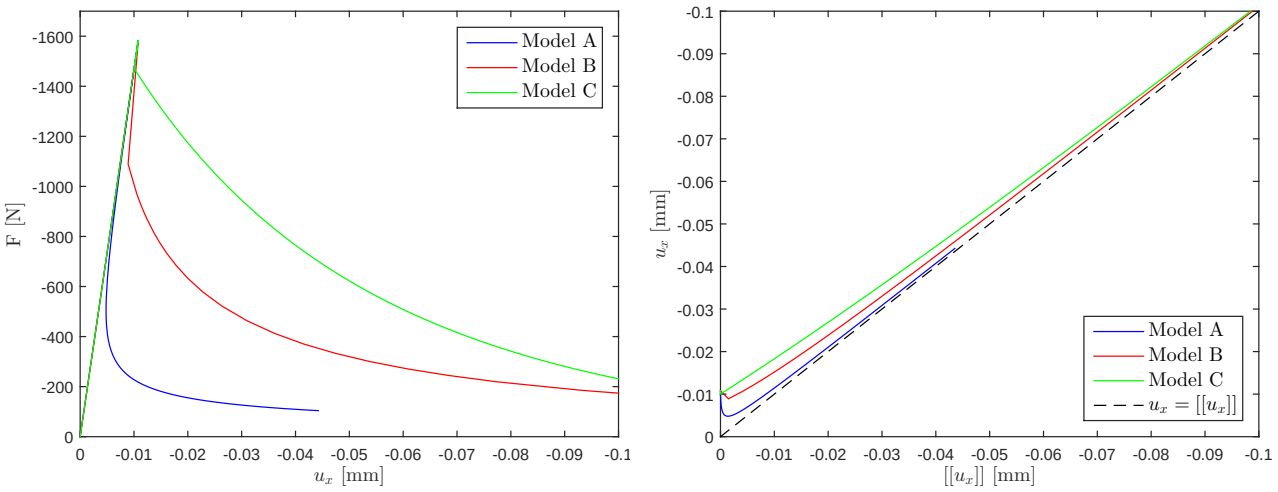

(a) (b)

Figure 4.4: (a) Load-displacement relations. (b) Axial displacement jump of models compared to total axial displacement.

The main goal of the analysis is to evaluate the failure response of the three models. As stated in section 3.1 prior to violation of the failure criteria the models behave linear elastic. Because the cohesive zone has not yet been inserted into the element at this point all three models follow the same pre-peak curve. This pre-peak branch of the response is therefore of little interest in the current analysis and will not be discussed further.

4.2.1. Load-displacement relation

The resulting load-displacement relation of the three models are presented in fig. 4.4a. It is immediately apparent that upon reaching σ_c all models suffer varying degrees of snap-back instability followed by a softening response. It can be seen that model A suffers the sharpest snap-back indicating that the elastic energy of the bulk material is quickly released after which the $u_x \rightarrow [\![u_x]\!]$ as can be observed in fig. 4.4b. Subsequently, the bulk material undergoes decreasing compression. At this point the collapse response of the model can directly be described by the response of the cohesive zone.

Model B suffers a less severe snap-back after reaching the limit load. Where commonly for kink bands a sharp snap-back is observed, here the response initially decreases discontinuously before transforming to a softening response. Furthermore, the elastic release is more gradual and u_x gradually approaches $[\![u_x]\!]$. It is interesting to note that while model B appears stiffer than model A when looking at the collapse response as a function of the transverse displacement (see fig. 4.5a) model B is the least stiff. In fact, by plotting the transverse displacement jump against the axial displacement jump (see fig. 4.5b) it can be observed that while the transverse deformation is the main deformation in models A and C, for model B the transverse displacements remains relatively small and the axial displacement jump steadily increases. This is both due to the fixation of the spring at a constant angle and the definition of $[\![\bar{u}_1]\!]$ which give greater influence to axial displacements.

Model C shows the least instability, with an exponentially softening response. This lack of instability is caused by the fact that the cohesive frame is fixed and is not constantly rotating causing a more stable load decrease. Here the response simply follows the damage function applied to the cohesive zone.

While model C exponentially decreases, both models A and B show load stabilization as failure progresses. This apparent stabilization is caused by the fact that damage is defined in

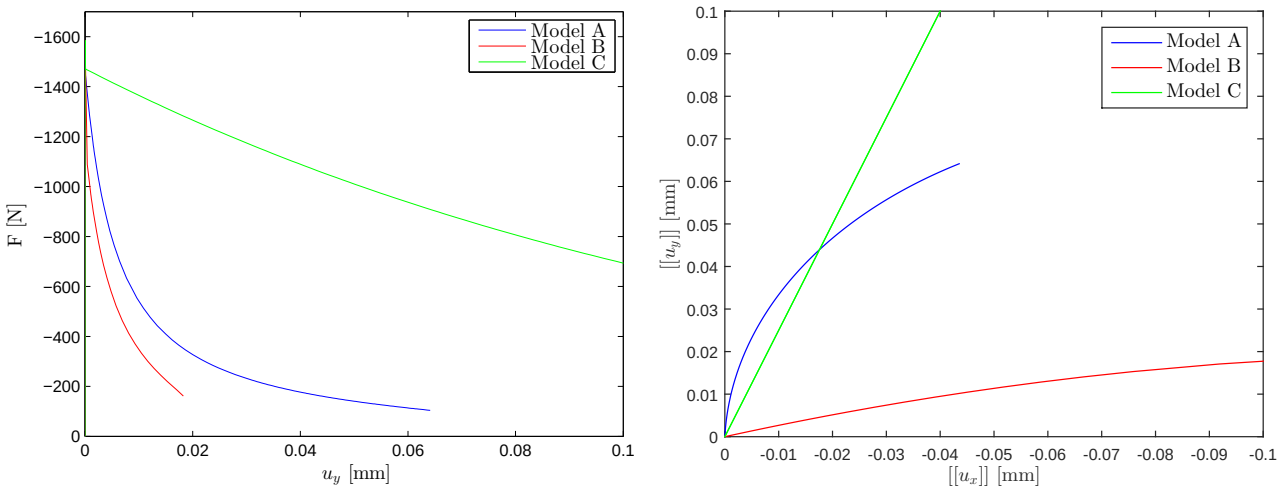

(a) (b)

Figure 4.5: (a) Load vs transverse displacement. (b) Transverse displacement jump against the axial displacement jump.

the local kink band frame and large displacements are needed to dissipate the high amount of energy attributed to $\bar{t}_2$.

4.2.2. Comparison Kinking theory

In order to asses the validity of the models, the collapse response is compared to the analytical solution derived by Budiansky and Fleck [4] for an ideally plastic matrix . The axial stress of the models is shown as a function of the fiber rotation in fig. 4.6 along with the analytical solution given by eq. (4.15).

$$\sigma = \frac{a\tau_y}{\alpha + \alpha_i} \tag{4.15}$$

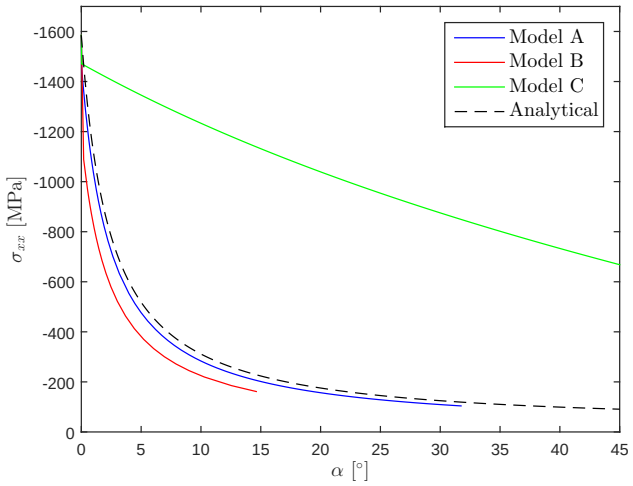

Figure 4.6: Axial stress vs fiber rotation

From fig. 4.6 it can be observed that with increasing fiber rotation both models A and B display the desired exponentially decreasing response. Both models A and B result in a slightly more conservative prediction then eq. (4.15) with model A in better agreement with eq. (4.15) than model B. The weaker response of model B is likely caused by the definition of $[\![\bar{\mathbf{u}}]\!]$. For enforcement of in-extensibility in model B the increase in transverse jump remains relatively small causing a slow development of α, while the axial stress steadily decreases.

As opposed to the other two models, model C shows no agreement with eq. (4.15). This poor compliance is caused by the omission of fiber rotation in the cohesive law. Due to the fixation of the angle by which the local traction is rotated to the global frame the response now becomes independent of fiber rotation and no longer bears any resemblance to the analytical solution.

Plasticity While model A shows good agreement with eq. (4.15) in the interest of a proper comparison it would be beneficial to exclude damage and assume that the matrix behaves ideally plastic as has been assumed for eq. (4.15). In this case it holds that $\bar{t}_2 = \bar{t}_2^f$ and $\hat{t}_s = \hat{t}_s^f$. It is clear that for model C this analysis will have no significance as model C is not influenced by fiber rotation and so the result of assuming $\hat{t}_s = \hat{t}_s^f$ is that the stress remains constant throughout the analysis.

The resulting curves are displayed in fig. 4.7. Here again a similar result is obtained as earlier, with model A showing the greater agreement with eq. (4.15). An interesting observation that can be made from this analysis is that for model A and B the plastic behavior appears to mimic the behavior seen when a damageable matrix is applied.

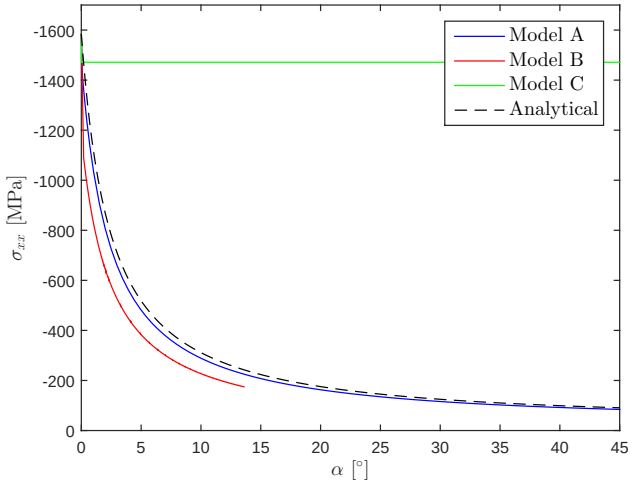

Figure 4.7: Axial stress vs fiber rotation for ideal plastic response

In fact, as can be seen in fig. 4.8, initially little to no difference is seen between the collapse response of an ideally plastic matrix and damageable matrix and as failure progresses the difference increases slightly. This indicates that the current damage formulation does not play an important role in the collapse response. In the current formulation the fracture energy is assumed to only be dissipated through cracking of the matrix. Consequently, a high amount of energy has to be dissipated, leading to a slow decrease of $\bar{t}_2$ and therefore little significance on the collapse response, especially in the early stages when the influence of $\bar{t}_2$ is limited due to the small angle α. The role of matrix cracking however should not be disregarded so quickly. In reality matrix cracks lead to decrease in stiffness and an increase in rotation causing steep decreases in the total resistance. The energy dissipated by matrix cracking however is not equal to G_{kink}. Various dissipative mechanisms are at work during kinking of which matrix cracking is one. Attributing G_{kink} only to the matrix leads to an overestimation of the matrix strength.

4.2.3. Closing remarks

Both models A and B show favorable results when compared to kinking theory response, however, suffer from a lack of robustness. Furthermore, while model B shows relative agreement with kinking theory, its behavior in axial direction and displacement field may be less than

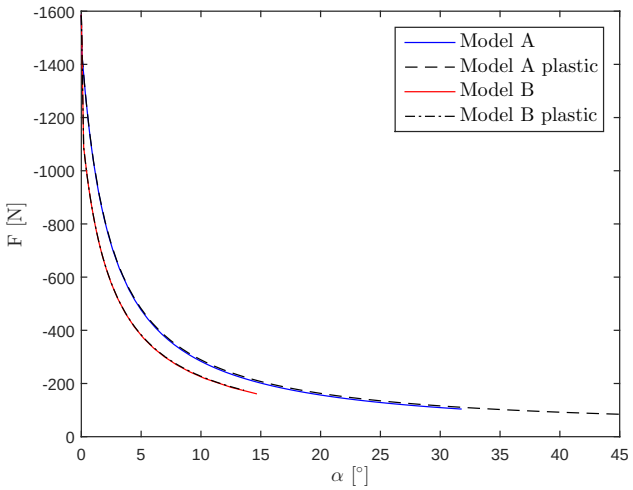

Figure 4.8: Axial stress vs fiber rotation for damageable and ideal plastic response

accurate. Kink band mainly deform in transverse direction while model B shows the main deformation to be in axial direction.

In contrast to models A and B, model C fails to show any agreement with the analytical solution. The lack of agreement can only be attributed to the omission of evolving fiber angle in the cohesive law. While for all models an in-extensibility clause is someway incorporated, the increasing fiber angle, caused by decreasing transverse stiffness, enables a rapid decrease in (global) axial stiffness which is not captured by model C.

Although computationally model C is the most robust it would still be of little use due to its inaccuracy. Therefore model C will not be addressed in the sensitivity analysis. Possible improvement of the model without losing much of its robustness would be to derive a more accurate damage function which readily incorporates the effects of the increasing fiber rotation angle.

4.3. Sensitivity analysis

Throughout the years the influence of various material parameters on fiber kinking has been evaluated. While many of these studies were focused on the influence to the failure load, analytical theories have shown that these may also hold significance when addressing the post-peak response. In particular, eq. (4.15) provides great insight into the influence of parameters such as; imperfection and yield strength on the post-peak behavior of the kink band.

Here the sensitivity of model A and B to several known influential factors of kinking is assessed. Model C is left out of this assessment due to its poor agreement with the analytical solution. Again comparison will be made between the models and kinking theory on a qualitative level. The main goal of these analysis is to asses if the analytical trends are captured by the model and therefore the focus is more on the cohesive zone response then on the failure behavior as a whole. Nonetheless when relevant the latter will be addressed.

4.3.1. Fiber misalignment

The fiber misalignment angle is a statistical parameter known to greatly influence the critical kinking stress. The hyperbolic relation between critical stress and α_i can directly be deduced from eq. (3.3). For the post-peak response however the influence of α_i is less significant. From eq. (4.15) it follows that initially while $\alpha_i \gg \alpha$ there is a strong influence of the misalignment angle, the initial response becomes less steep with increasing α_i. However, as can be seen in

fig. 4.9 as α continuously increases the influence of the misalignment angle disappears and the failure responses converge.

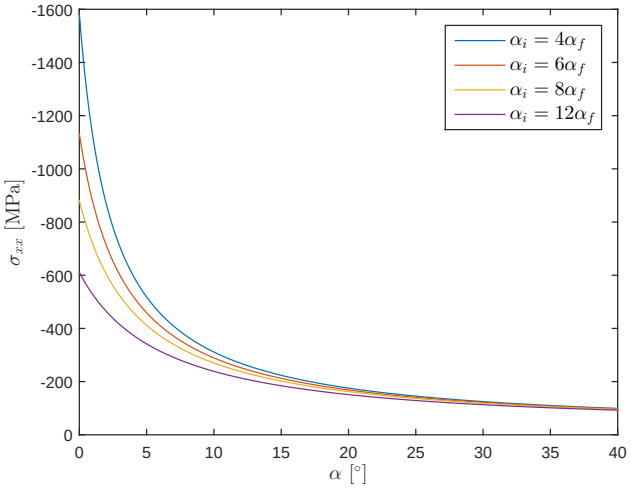

Figure 4.9: Failure response of kinking theory for different values of fiber misalignment.

Both from the analytical solution and from the physics of fiber kinking one can deduce that the initial misalignment angle will be most influential in the early stages of failure of the kink band. This phenomenon is captured well by both models as can be seen in fig. 4.10. It can be observed that both models exhibit a similar sensitivity to the increasing misalignment angle with model B showing faster convergence of the cohesive traction. This is likely caused by the fact that the local traction components of model B are independent functions of their respective displacement jump. Because in the later stages the role of $\bar{t}_2$ becomes more significant, the fact that for model A this is not only a function of $[\![\bar{u}_2]\!]$ (and therefore α) may cause an increased response as can be seen for $\alpha_i = 4\alpha_f$.

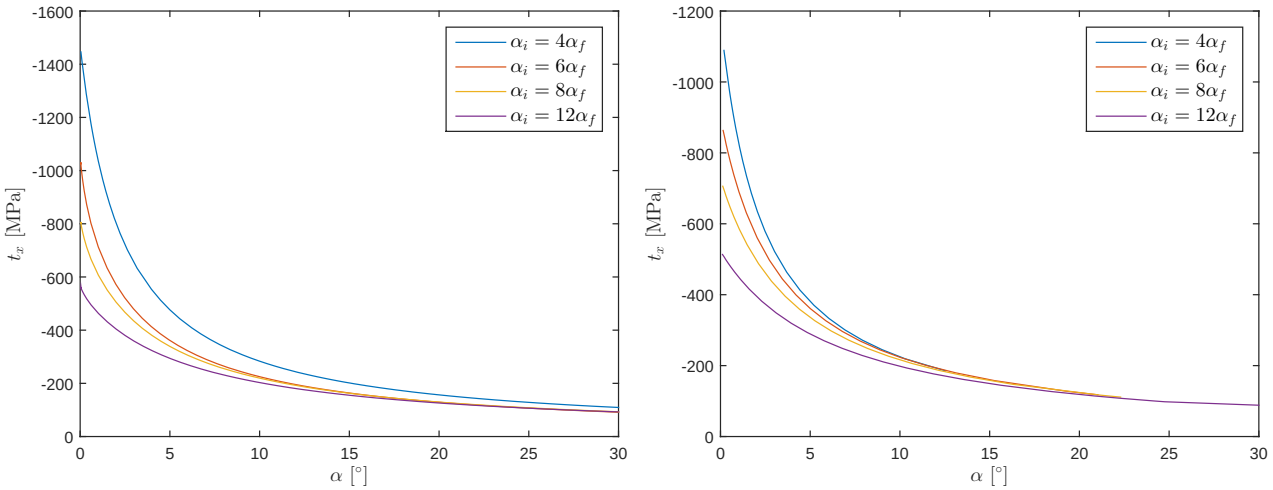

(a) (b)

Figure 4.10: Axial traction vs fiber rotation for varying α_i: (a) Model A. (b) Model B.

By looking at the load-displacement relation (see fig. 4.11) one can see the effect of the misalignment angle on the global structural behavior. Clearly the effect on critical stress is captured by the failure criteria which is equal for both models. Furthermore, both models show a decreasing snap-back caused by the lower critical stress which ultimately at unrealistic values of the misalignment angle will disappear completely. The difference between the models is also much more visible. While model A shows little effect of the varying α_i in the post-peak response, model B shows a higher variation in the initial post-peak response.

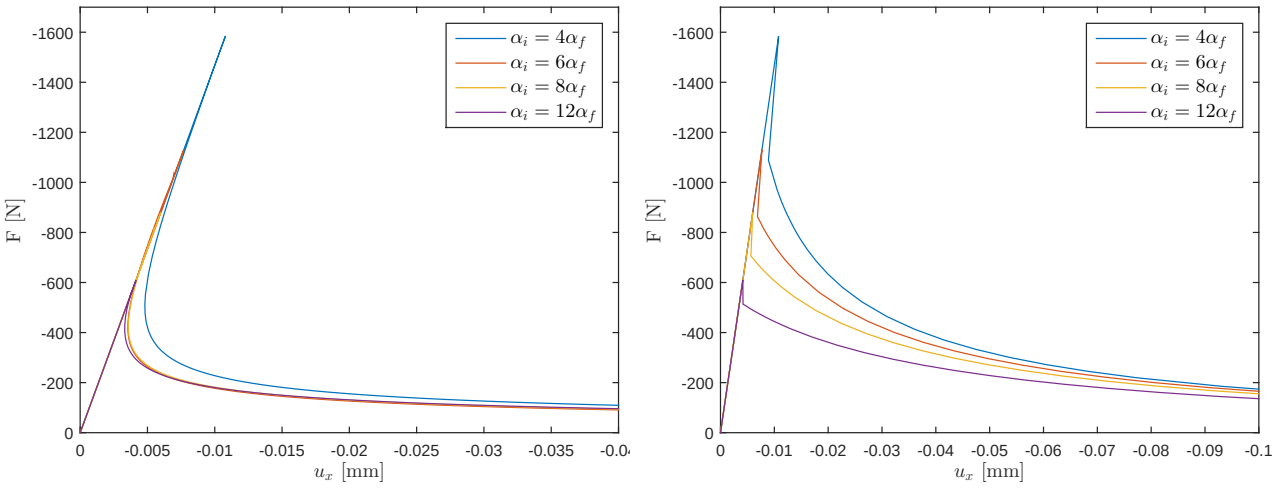

Figure 4.11: Collapse response for varying α_i: (a) Model A. (b) Model B.

Considering the physics of fiber kinking one can argue that, while the misalignment angle has serious consequences for the global failure load the stiffness and resistance to rotation is not affected. Indeed there will be a slight increase in the ϕ_f angle and therefore heightened influence of the matrix behavior, however, the matrix behavior itself is not affected. Furthermore, the bulk material remains unchanged. This all indicates that the misalignment angle should not have much influence on the failure behavior at the global level, making the predictions of model A the more realistic of the two.

4.3.2. Shear yield strength

The yield strength or failure strength of the matrix is linearly related to the kink band failure load. Other then its relation to the kink band strength, the yield strength has limited influence on the post-peak behavior causing only an increase in the kink band response for increasing yield strength. Both in an analytical and physical sense it is obvious that an increase in matrix strength will cause an increase in the post peak response and cause that the resulting stress-rotation relations are simply vertical translations of each other as can be seen in fig. 4.12.

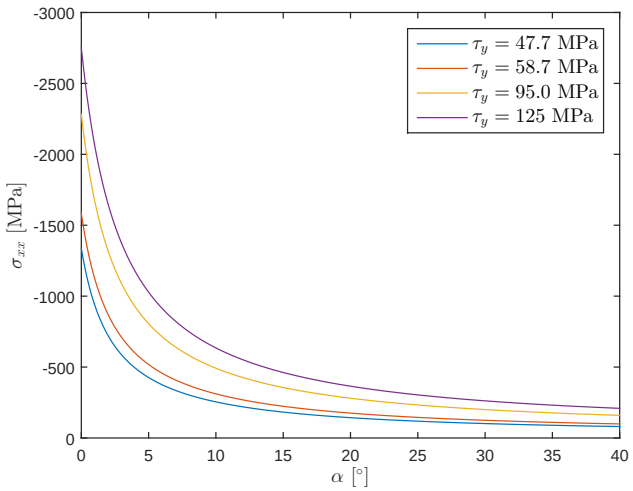

Figure 4.12: Failure response of kinking theory for different values of yield strenght.

This effect is well captured by both model A and B as can be seen in fig. 4.13. Both models

show the increase in the cohesive response with increasing yield strength and no further change to their post-peak behavior. With respect to the sensitivity to shear strength the models are equivalent for both local as global behavior.

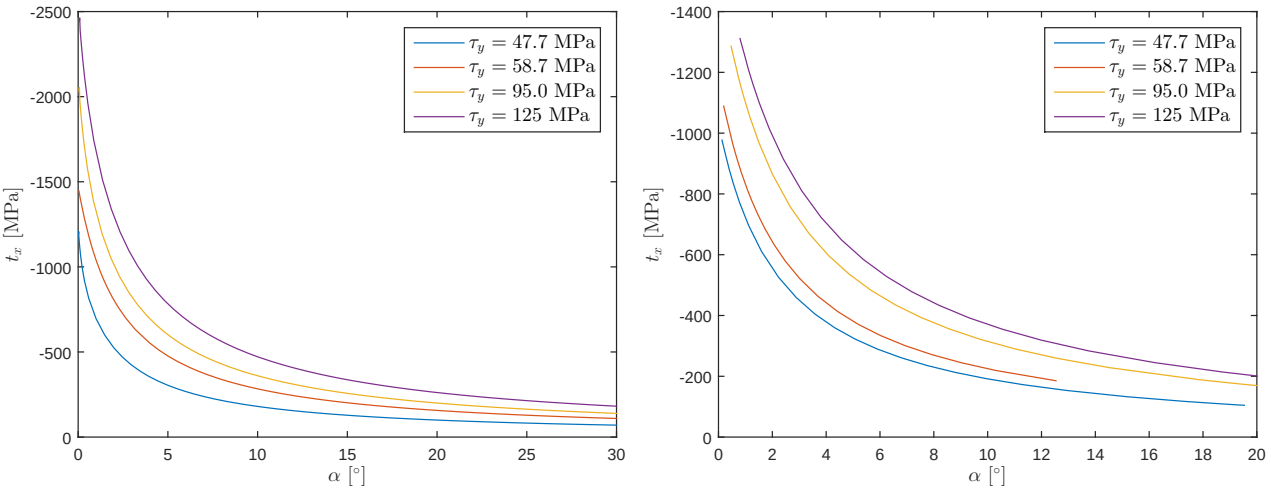

(a) (b)

Figure 4.13: Axial traction vs fiber rotation for varying τ_y: (a) Model A. (b) Model B.

An interesting observation that can be made from model B is that with increasing strength, the initial rotation angle of the post-failure solution also increases. This is due to the definition of $\bar{K}_{22}$:

$$\bar{K}_{22} = \frac{\bar{t}_2^f}{[\![\bar{u}_2]\!]_f} = \frac{\frac{a\tau_y}{\alpha_i+\alpha_f}\sin(\alpha_i)}{w\alpha_f} = \frac{\frac{a\tau_y}{\alpha_i+\frac{tau_y}{aG}}}{w\frac{\tau_y}{aG}}\sin(\alpha_i) = \frac{a^2G}{w\left(\alpha_i+\frac{\tau_y}{aG}\right)}\sin(\alpha_i) \tag{4.16}$$

which shows that for increasing yield strength $\bar{K}_{22}$ will decreases. From a physical point of view it is unlikely that the yield strength will have any influence on the matrix stiffness as a stronger matrix does not necessarily imply a stiffer matrix. Therefore the definition of $\bar{K}_{22}$ has the drawback that it implies an unnatural relation between strength and stiffness.

4.3.3. Shear stiffness

The influence of the shear stiffness can also be derived from the analytical solution. From the analytical solution it follows that, similarly to the fiber misalignment angle, the shear stiffness only greatly influences the initial stages of kinking as can be seen fig. 4.14. This behavior is captured well by model B (see fig. 4.15b), were eq. (4.16) can be used to show the relation between G and K_{22} and explain the increase in the initial angle α for decreasing G.

Model A however shows a different behavior (see fig. 4.15a), counterintuitively the post-peak strength appears to increase for decreasing values of G. This may possibly be a caused by the definition of kink band stiffness matrix $\bar{\mathbf{K}}^{\mathbf{e}}$. Because the acoustic tensor is used as the stiffness, the shear stiffness appears also in the off-diagonal terms of the matrix $\bar{\mathbf{K}}^{\mathbf{e}}$. Furthermore, because $[\![\bar{v}_1]\!]$ is negative and $[\![\bar{v}_2]\!]$ is positive, a decrease of the shear stiffness (and therefore the off-diagonal terms) could cause the observed increase in the traction. However, because $[\![\bar{v}_1]\!] \to 0$ it is uncertain if $\bar{\mathbf{K}}^{\mathbf{e}}$ is truly the cause. Moreover the question also arises whether the behavior shown by model A is truly incorrect.

In the case of matrix stiffness comparing both models to just the analytical solution is not sufficient to asses their validity. The analytical solution used here assumes ideal plasticity and therefore assumes that matrix stiffness has no influence in post-peak response. However, it can be expected that the matrix stiffness will indeed effect the post-peak response as it directly

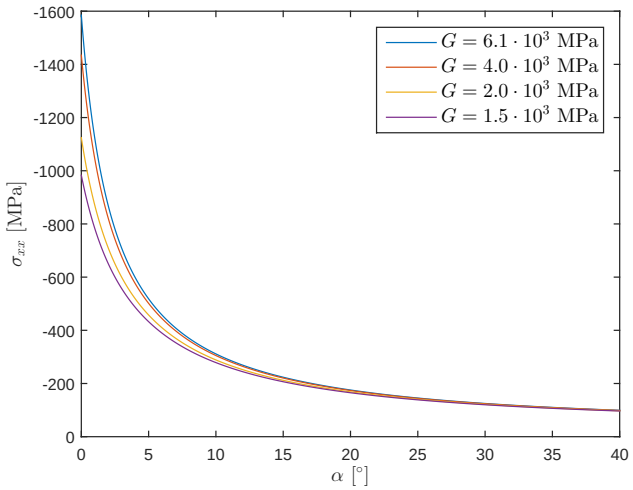

Figure 4.14: Analytical collapse response for varying values of G.

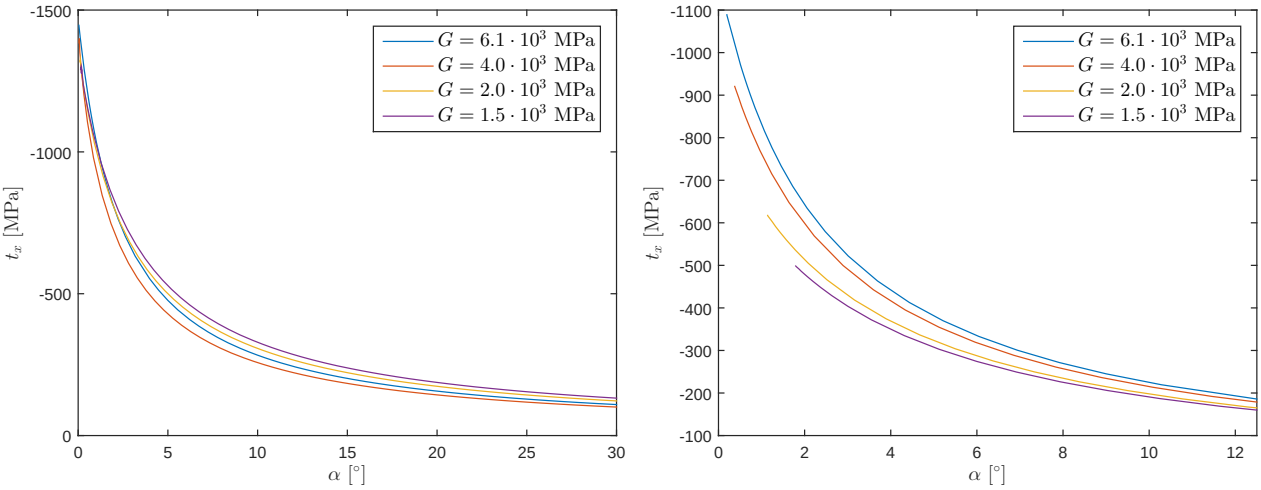

(a) (b)

Figure 4.15: Axial traction vs fiber rotation for varying G: (a) Model A. (b) Model B.

relates to the composites resistance to fiber rotation. When looking at other analysis of kinking that consider strain hardening type matrices [9, 28] the influence of shear stiffness in the post-peak response becomes apparent. A direct relation between shear stiffness and and post-peak response is however not simple to deduce. Furthermore, it is likely that the ratio between shear and transverse stiffness also plays a role in the post-peak response making it all the more difficult to truly evaluate which model predicts the correct sensitivity.

What can be said however, is that because model B does not directly incorporate the matrix stiffness and, as pointed out by eq. (4.16), $\bar{K}_{22}$ is also a function of the strength, it is unlikely that model B provides a good approximation of the real sensitivity. This omission of the stiffness parameters also explains why model B shows good agreement with the ideally plastic analytical solution.

4.3.4. Finite fiber stiffness

Throughout this thesis it has been constantly assumed that fibers within the kink band are infinitely stiff in axial direction. While this assumption allowed for various simplifications it is unclear whether a finite stiffness had great influence on the response. Budiansky and Fleck have addressed this issue in their derivation of kinking theory [4]. However they only focused on the effects on the critical stress providing little insight into the effects on the collapse response.

For that reason here the influence of varying levels of axial stiffness for the kink band will be compared to the infinitely stiff case in order to asses the validity of the infinite stiffness assumption. It is worth noting that now $E_{11} \neq \infty$ and subsequently, $\bar{K}_{11} \neq \infty$, the same damage function is used with the assumption that $[\![\bar{v}_1]\!] \to 0$.

The collapse responses are depicted in fig. 4.16 as a function of α. As can be observed, there is no significant change in the response of model B for the varying E_{11}, which validates the assumption of in-extensible fibers for that model. Model A however shows a clear influence of the axial stiffness on the collapse response, with a decreasing capacity for decreasing values of E_{11}. However, ultimately as failure progresses the responses seem to converge to an equal path.

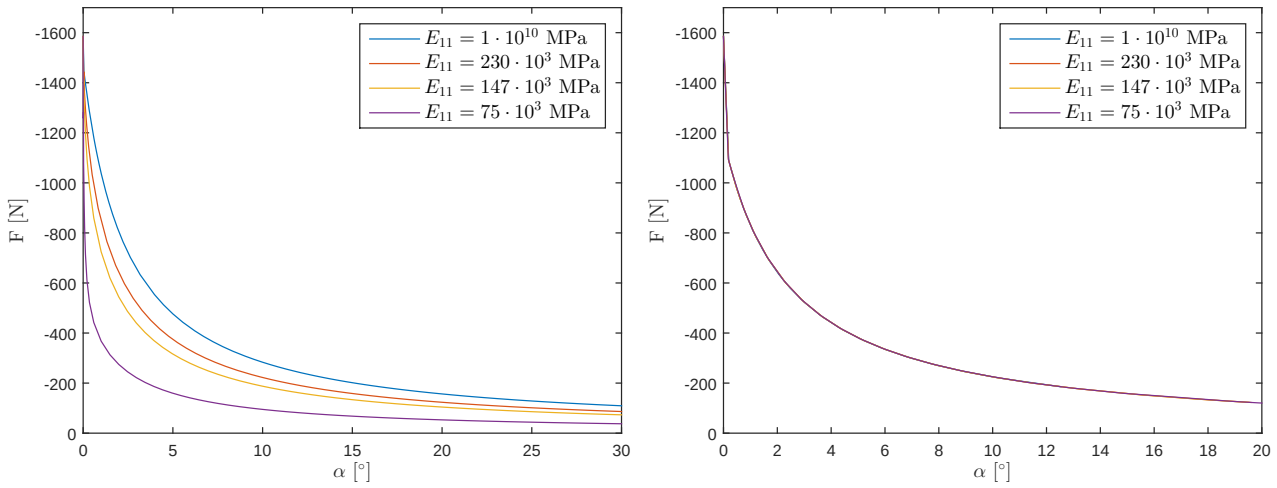

Figure 4.16: Collapse response for varying E_{11}: (a) Model A. (b) Model B.

By plotting the local axial displacement $[\![\bar{v}_1]\!]$ against the fiber rotation one can asses whether the assumption $[\![\bar{v}_1]\!] \to 0$ used in deriving the damage scaling parameter A still remains valid. From fig. 4.17 it can be observed that initially $[\![\bar{v}_1]\!]$ increases substantially. For model B it is observed that initially $[\![\bar{v}_1]\!]$ is negative but as the fiber rotate $[\![\bar{v}_1]\!] \to 0$ validating the assumption made earlier during derivation. Similarly for model A, $[\![\bar{v}_1]\!]$ is initially negative however in this case as rotation increases the value of $[\![\bar{v}_1]\!]$ switches sign indicating extension of the kink band. The local axial traction however still remains negative due to its relation to $[\![\bar{v}_2]\!]$. This means that for model A, while $[\![\bar{v}_1]\!]$ remain relatively small it can no longer be assumed that $[\![\bar{v}_1]\!] \to 0$ and consequently eq. (3.29) is no longer valid.

A clear difference can be seen between model A and B with respect to their sensitivity to the axial stiffness. while no significant effect are seen on the collapse response and evolution of $[\![\bar{v}_1]\!]$ of model B this is not the case for model A. The explanation for this is twofold. Firstly, for model B, $[\![\bar{u}_1]\!]$ is defined from a buckling perspective while in model A, $[\![\bar{u}_1]\!]$ follows from rotation. By definition model A therefore allows easier growth of $[\![\bar{u}_1]\!]$. Additionally, the definition of $\bar{\mathbf{K}}$ for model A implies an increased influence of $[\![\bar{u}_1]\!]$ in the collapse response. Both these factor imply an increased influence of E_{11}.

The question now remains whether or not the kink band response is truly influenced by E_{11}. While many texts on the subject of kinking have assumed in-extensible fibers, one could still argue that the main deformations within the band are fiber rotation and matrix shearing. Furthermore, considering the usually high axial stiffness of composites, it is hard to imagine that there is significant compression or extension of the band that greatly influences the post peak response, especially in the later stages of kinking.

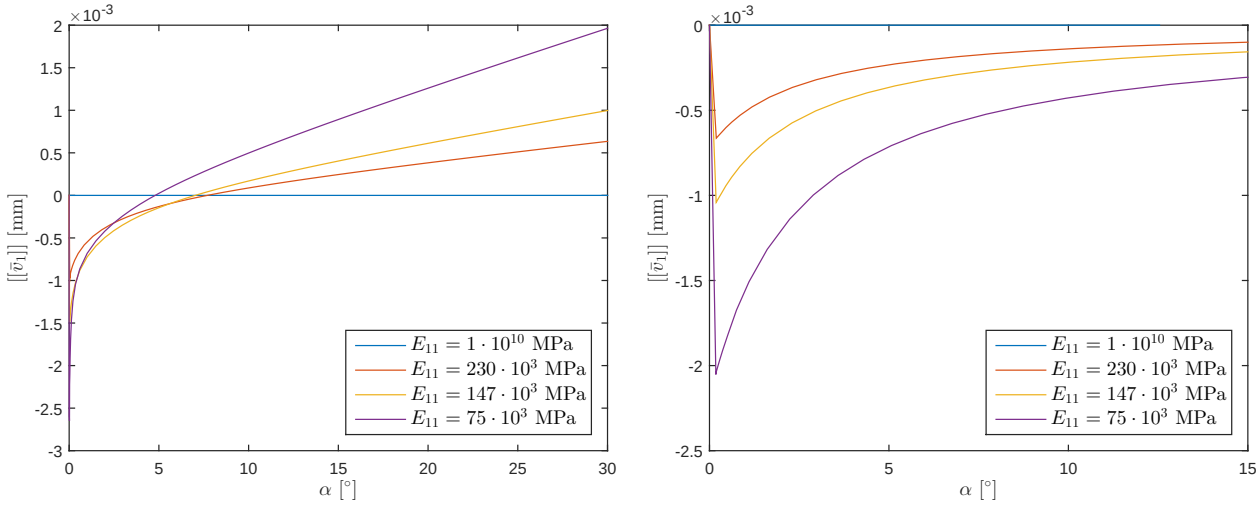

Figure 4.17: Collapse response for varying E_{11}: (a) Model A. (b) Model B.

4.4. Discussion

The three models have been implemented and compared to the well known kinking theory solution of Budiansky and Fleck [4]. The sensitivity of models A and B have also been addressed, while model C was omitted due to its poor agreement with kinking theory. It is now important to discuss the workings of the models and classify them based on their accuracy, efficiency and robustness. In this section these aspects are briefly discussed in order to determine the models suitability for analysis of fiber kinking.

4.4.1. Model A

The collapse response of model A has shown to be in good agreement with kinking theory and gives a realistic prediction for the behavior of kink bands. From the sensitivity analysis it can also be seen that model A performs admirably and is capable of capturing sensitivities that effect kink bands. Because of the explicit presence of the kink band constitutive matrix in the cohesive model it can be expected that model A is capable of accounting for various material properties that may influence kinking and can be used to study these effects. To that end further improvements in the constitutive description of kink bands can be readily incorporated in the model by modification of the $\bar{\mathbf{D}}$-matrix. A drawback however of using the strong discontinuity analysis is the presence of off-diagonal terms in the cohesive stiffness matrix, which imply an influence of $[\![\bar{u}_1]\!]$ where micro-mechanically speaking only α (and therefore $[\![\bar{u}_2]\!]$) is significant.

Computationally there is also an issue that requires further discussion. It would not have escaped the readers attention that model A is terminated prematurely. This is caused by the fact that model A requires relatively small step sizes for fast convergence, even when the load has somewhat stabilized. Ultimately, the minimum arclength and maximum number of iteration is reached and the algorithm is terminated. However, when no restriction is implemented on the number of iterations the system continues to converge upto and beyond $\alpha = 45°$. Beyond $\alpha = 45°$ the resulting predictions are of little interest, as realistic rotation angles do not reach this value prior to complete collapse of the specimen. For model A this is not the case due to the high fracture energy attributed to the matrix.

4.4.2. Model B

Similar to model A, model B also gives relatively good agreement when compared to kinking theory, however, the predicted ratio between axial- and transverse displacement is inaccurate and not representative of reality. Sensitivity analysis similarly revealed that although there is a good agreement with kinking theory, model B is only sensitive to parameters influencing the critical kinking stress and can not be used to asses other parameters such as transverse stiffness. Furthermore the definition of $\bar{K}_{22}$ implies strength properties influence the stiffness which is unrealistic. Re-derivation of $\bar{K}_{22}$ starting from the stress-strain-displacement relation would alleviate this issue and allow for a better sensitivity behavior. However, the inaccuracies in displacements are a direct result of the modeling approach and cannot be mitigated.

Computationally the model also has deficiencies. Initially model B has a good convergence behavior requiring only a few iterations for relatively large step sizes. However, ultimately the model suddenly fails to converge for all admissible step sizes while $\alpha \ll 45°$. Even when the maximum number of iterations is increased convergence does not continue long before the solution diverges. Unfortunately, it is unclear what causes the divergence and therefore no remedy could be found for this problem.

4.4.3. Model C

Model C showed no agreement with kinking theory and therefore was not addressed in the sensitivity analysis. One can however argue that as the stiffness is derived in a similar fashion to model B, model C will most likely show similar sensitivities as model B, being only influenced by parameters that effect the kinking stress.

Computationally model C was the most efficient due to its simplistic formulation, however, this is of little significance considering its poor prediction. It is however worth stating that model C did serve great purpose as it confirms the assumption that the rotating kink band frame rotation is the dominant factor in kink band response. To that end one may be able to achieve better accuracy if the effects of fiber rotating could be included in the damage function of model C and allowing damage in normal direction even for compression.

4.4.4. Closing remarks

It is clear from the preceding sections that out of the three models, model A provides the most accurate results with a realistic prediction of the failure behavior. Model A should therefore be considered further for future analysis and further improvement.

Both models B and C ultimately result in some form of unrealistic prediction. For model B it would be of little benefit to further develop the model and improve the issues mentioned as the main issue is rooted in the modeling approach itself.

Improvements may be possible for model C, however, in the current implementation the improved computational behavior of model C is of little consequence and improvement of this model will not be beneficial as model A already provides accurate results. When more complex analysis are attempted where robustness and efficiency plays an increasing role it may be beneficial to re-evaluate the need for a computationally simplistic model.

Chapter 5: Conclusions and recommendations

5.1. Conclusions

In this work a computational model for fiber kinking has been developed. Kink bands are modeled as mesh-independent discontinuities that arise after violation of a failure criterion using the phantom node method. Three cohesive models were derived for simulation of the collapse response of the kink band. The response of the models were tested and compared to the analytical kinking theory response proposed by Budiansky and Fleck [4]. The main conclusions of the analysis are:

1. The discontinuous approach can be used to model kink bands with relative accuracy provided a proper cohesive model is used.

2. The fiber rotation angle must be included in the cohesive zone model in order to arrive at an accurate prediction of the collapse response. A simple formulation that ignores the constant change of the rotation matrix (model C) can not properly account for the rapid decrease in capacity. A possible solution could be derivation of a damage law that directly incorporates the effects of fiber rotation on the material response.

3. A discrete damage formulation affecting only the resistance to fiber rotation can be used to account for different types of matrices (ductile or brittle). However, attribution of the total kink band fracture energy to matrix cracking is inaccurate and results in over-prediction of the resistance to fiber rotation. Accurate description of the dissipative mechanisms is needed to derive a proper distribution of fracture energy and improve the damage formulation.

4. The strong discontinuity model (model A) present a favorable way of incorporating the continuum constitutive behavior of kink bands in a cohesive model. In terms of accuracy, sensitivity and capacity for further improvement, model A outperforms the other models considered in this thesis and provides a realistic prediction of the composite behavior when subjected to kinking. Model A is therefore to be preferred for further analysis.

5.1.1. Reflection on goal and objectives

Considering the goal of this thesis a computational model has been developed to simulate fiber kinking failure of composite laminates. Three mechanical models for kink bands have been introduced and the necessary mathematical formulations have been derived and qualitatively assessed using a one dimensional numerical framework. In that respect the goal and objectives of this thesis have been achieved. Furthermore, the model that has been derived is such that it can be readily implemented into a two dimensional numerical framework for further validation.

The research question can be answered in the following manner:

Failure by fiber kinking can be incorporated in a meso-level computational model for composite laminates by modeling kink bands as mesh independent discontinuities with an appropriate cohesive model that incorporates the characteristic kink band behavior.

5.2. Recommendations

The work in this thesis was limited to pure axial compressive loading of a one dimensional beam element. Based on the analysis several recommendations for future analysis and improvement of model can be made.

The recommendations made here only relate to model A as this model has provided the most realistic depiction of the kink band response and sensitivity. It is however, still worth mentioning that possible improvement in the behavior of model C can be achieved by implementation of a damage law that can incorporate effects of fiber rotation to both the normal and shear traction components.

5.2.1. Future analysis

First and foremost the model should be extended to a 2D framework and verified against experimental or numerical[1] data. The model developed can be readily implemented in a 2D framework and is capable of handling failure propagation. Some algorithmic aspects such as; the arclength method and adaptive time stepping scheme, will however require adjustment in order to maintain their efficiency in the 2D framework. In the two dimensional framework the model can further be tested under multi-axial loading and interaction with other failure mechanisms.

Further extension to 3D may not be warranted as experimentation usually constrains the specimens such that only in-plane or out of plane kinking occurs therefore it is, to the best of the authors knowledge, uncertain how the fracture plane in a full 3D test develops. In this situation the failure criteria must be adapted to a 3D situation where the propagation angle and fracture plane follow from the stress state and constraints (such as other plies etc.). Furthermore the validity of the cohesive models needs to be re-evaluated as kinking theory has been derived based on a 2D stress state and the validity of the infinite band assumption has not been proven in 3D.

5.2.2. Model Improvement

As previously mentioned to improve model A it may be beneficial to make use of a diagonal $\bar{\mathbf{K}}^{\mathbf{e}}$-matrix instead of the elastic acoustic tensor. In this case the $\bar{t}_1$ component will then only be dependent on axial displacements and the $\bar{t}_2$ component on transverse displacement (and therefor α). Care must be taken in deriving this relation, the simplified method used in determining the stiffness of model B and C should be avoided as it results in unrealistic dependencies. $\bar{\mathbf{K}}^{\mathbf{e}}$ should be derived directly from the stress-strain-displacement relation.

Another approach that might be useful is to determine the kink band strains directly from the displacement jump and rotation angle instead of transforming the continuum description to a discrete one. From here the constitutive relation (be it plasticity or damage) can directly be applied to determine the kink band stresses. Using then the same transformation as used in section 3.2.2 the traction and tangent can be determined. This provides the additional

[1] Micro-mechanical finite element analysis.

advantage that existing constitutive relations can be readily used without the need to transform them to a discrete setting.

5.2.3. Model expansion

For the cohesive zone modeling the assumption was made that only the matrix plays a role in failure and fiber bending resistance was ignored along with strains and deformations of the fiber. Although this assumption is accurate in predicting the failure load, fiber failure does contribute to energy dissipation. Therefore inclusion of energy dissipation via fiber failure would give a better representation of reality and improve the models accuracy. More research is however required in order to complement current knowledge on the fracture mechanistic aspects of kink bands. In particular more knowledge is required on the dissipative mechanisms at work, interaction between these mechanisms and proper characterization of this process.

A further expansion of the model would be inclusion of the band broadening phenomenon. Although a discontinuous approach is used where the kink band width is not physically represented, band broadening can still be included in the cohesive law by taking into account volumetric lock-up of the matrix and increase of the kink band width.

In addition to broadening, the effects of an evolving band angle can also be considered. In the current model the kink band propagation angle (β) is assumed fixed and no considerations are made to the initially evolving state of β. When propagation is addressed in a 2 or 3 dimensional setting it is possible to account for the initially evolving β by determining the β-angle for each failed element when the failure criterion is violated. This would require a formula to determine β for each failed element. Such a formula is, to the best of the authors knowledge, not readily available. Therefore more research is needed for proper understanding of the development of propagation angle.

Bibliography

[1] A. Argon. Fracture of composites. In H. HERMAN, editor, *Treatise on Materials Science & Technology*, volume 1 of *Treatise on Materials Science & Technology*, pages 79 – 114. Academic Press, New York, 1972.

[2] Z. Bažant, J.-J. Kim, I. Daniel, E. Becq-Giraudon, and G. Zi. Size effect on compression strength of fiber composites failing by kink band propagation. In Z. Bažant and Y. Rajapakse, editors, *Fracture Scaling*, pages 103–141. Springer Netherlands, 1999.

[3] B. Budiansky. Micromechanics. *Computers & Structures*, 16(1–4):3 – 12, 1983.

[4] B. Budiansky and N. Fleck. Compressive failure of fibre composites. *Journal of the Mechanics and Physics of Solids*, 41(1):183 – 211, 1993.

[5] B. Budiansky, N. Fleck, and J. Amazigo. On kink-band propagation in fiber composites. *Journal of the Mechanics and Physics of Solids*, 46(9):1637 – 1653, 1998.

[6] P. Davidson and A. M. Waas. Mechanics of kinking in fiber-reinforced composites under compressive loading. *Mathematics and Mechanics of Solids*, May 2014.

[7] C. Dávila, N. Jaunky, and S. Goswami. Failure criteria for frp laminates in plane stress. In *44th AIAA/ASME/ASCE/AHS/ASC Structures, Structural Dynamics, and Materials Conference*. American Institute of Aeronautics and Astronautics, Apr 2003.

[8] R. de Borst. Computation of post-bifurcation and post-failure behavior of strain-softening solids. *Computers & Structures*, 25(2):211 – 224, 1987.

[9] N. Fleck. Compressive failure of fiber composites. In J. W. Hutchinson and T. Y. Wu, editors, *Advances in Applied Mechanics*, volume 33 of *Advances in Applied Mechanics*, pages 43 – 117. Elsevier, 1997.

[10] N. A. Fleck, L. Deng, and B. Budiansky. Prediction of kink width in compressed fiber composites. *Journal of Applied Mechanics*, 62(2):329 – 337, Jun 1995.

[11] N. A. Fleck and J. Y. Shu. Microbuckle initiation in fibre composites : A finite element study. *Journal of the Mechanics and Physics of Solids*, 43(12):1887 – 1918, 1995.

[12] R. Gutkin, S. Pinho, P. Robinson, and P. Curtis. On the transition from shear-driven fibre compressive failure to fibre kinking in notched cfrp laminates under longitudinal compression. *Composites Science and Technology*, 70(8):1223 – 1231, Aug 2010.

[13] R. Gutkin, S. Pinho, P. Robinson, and P. Curtis. A finite fracture mechanics formulation to predict fibre kinking and splitting in cfrp under combined longitudinal compression and in-plane shear. *Mechanics of Materials*, 43(11):730 – 739, Aug 2011.

[14] A. Hansbo and P. Hansbo. A finite element method for the simulation of strong and weak discontinuities in solid mechanics. *Computer Methods in Applied Mechanics and Engineering*, 193(33-35):3523–3540, Aug 2004.

[15] S. Kyriakides, R. Arseculeratne, E. Perry, and K. Liechti. On the compressive failure of fiber reinforced composites. *International Journal of Solids and Structures*, 32(6–7):689 – 738, 1995. Time Dependent Problems in Mechanics.

[16] P. Maimí, P. Camanho, J. Mayugo, and C. Dávila. A continuum damage model for composite laminates: Part i – constitutive model. *Mechanics of Materials*, 39(10):897–908, Oct 2007.

[17] P. Maimí, P. Camanho, J. Mayugo, and C. Dávila. A continuum damage model for composite laminates: Part ii – computational implementation and validation. *Mechanics of Materials*, 39(10):909–919, Oct 2007.

[18] P. M. Moran, X. H. Liu, and C. F. Shih. Kink band formation and band broadening in fiber composites under compressiove loading. *Acta Metallurgica et Materialia*, 43(8):2943 – 2958, Aug 1995.

[19] N. Naik and R. S. Kumar. Compressive strength of unidirectional composites: evaluation and comparison of prediction models. *Composite Structures*, 46(3):299 – 308, 1999.

[20] K. Niu and R. Talreja. Modeling of compressive failure in fiber reinforced composites. *International Journal of Solids and Structures*, 37(17):2405 – 2428, 2000.

[21] J. Oliver. On the discrete constitutive models induced by strong discontinuity kinematics and continuum constitutive equations. *International Journal of Solids and Structures*, 37(48–50):7207 – 7229, 2000.

[22] S. Pimenta, R. Gutkin, S. Pinho, and P. Robinson. A micromechanical model for kink-band formation: Part I experimental study and numerical modelling. *Composites Science and Technology*, 69(7-8):948 – 955, Jun 2009.

[23] S. Pimenta, R. Gutkin, S. Pinho, and P. Robinson. A micromechanical model for kink-band formation: Part II analytical modelling. *Composites Science and Technology*, 69(7-8):956 – 964, Jun 2009.

[24] S. Pinho. *Modelling failure of laminated composites using physically-based failure models*. PhD thesis, Imperial College London, 2005.

[25] S. Pinho, R. Gutkin, S. Pimenta, N. D. Carvalho, and P. Robinson. 7 - fibre-dominated compressive failure in polymer matrix composites. In P. Robinson, E. Greenhalgh, and S. Pinho, editors, *Failure Mechanisms in Polymer Matrix Composites*, Woodhead Publishing Series in Composites Science and Engineering, pages 183 – 223. Woodhead Publishing, 2012.

[26] V. W. Rosen. Mechanics of composite strengthening. In *Fiber Composite Materials*, pages 37 – 75. American Society of Metals, Metals Park, Ohio, 1965.

[27] C. R. Schultheisz and A. M. Waas. Compressive failure of composites, part i: Testing and micromechanical theories. *Progress in Aerospace Sciences*, 32(1):1 – 42, 1996.

[28] W. Slaughter, N. Fleck, and B. Budiansky. Compressive failure of fiber composites: the roles of multiaxial loading and creep. *Journal of engineering materials and technology*, 115(3):308–313, 1993.

[29] K. D. Sørensen, L. P. Mikkelsen, and H. M. Jensen. On the simulation of kink bands in fiber reinforced composites. In *28th Risø International Symposium on Materials Science: Interface Design of Polymer Matrix Composites-Mechanics, Chemistry, Modelling and Manufacturing*, pages 281–288, 2007.

[30] M. Sutcliffe and N. Fleck. Microbuckle propagation in fibre composites. *Acta Materialia*, 45(3):921 – 932, 1997.

[31] F. P. van der Meer. *Computational modeling of failure in composite and laminates*. PhD thesis, Delft University of Technology, 2010.

[32] A. M. Waas and C. R. Schultheisz. Compressive failure of composites, part ii: Experimental studies. *Progress in Aerospace Sciences*, 32(1):43 – 78, 1996.

[33] O. C. Zienkiewicz, R. L. Taylor, and J. Zhu. *The Finite Element Method : ITS Basis and Fundamentals*. Butterworth-Heinemann, 7th edition, 2005.